Nonplanar ground states of frustrated antiferromagnets on an octahedral lattice

Sophia R. Sklan[1,2] and Christopher L. Henley[1]

[1]*Laboratory of Atomic and Solid State Physics, Cornell University, Ithaca, New York, 14853-2501*
[2]*Department of Physics, Massachusetts Institute of Technology, Cambridge, Massachusetts 02139*

We consider methods to identify the classical ground state for an exchange-coupled Heisenberg antiferromagnet on a non-Bravais lattice with interactions J_{ij} to several neighbor distances. Here we apply this to the unusual "octahedral" lattice in which spins sit on the edge midpoints of a simple cubic lattice. Our approach is informed by the eigenvectors of J_{ij} with largest eigenvalues. We discovered two families of non-coplanar states: (i) two kinds of commensurate state with cubic symmetry, each having twelve sublattices with spins pointing in (1,1,0) directions in spin space (modulo a global rotation); (ii) varieties of incommensurate conic spiral. The latter family is addressed by projecting the three-dimensional lattice to a one-dimensional chain, with a basis of two (or more) sites per unit cell.

I. INTRODUCTION

This paper concerns the classical ground state of the Hamiltonian

$$\mathcal{H} = \sum_{ij} -J_{ij}\mathbf{s}_i \cdot \mathbf{s}_j \qquad (1.1)$$

where $\{\mathbf{s}_i\}$ are unit vectors, and the couplings $\{J_{ij}\}$ have the symmetry of the lattice and may extend several neighbors away (being frustrated in the interesting cases).

After an antiferromagnet's ordering pattern (or partial information) is determined by neutron diffraction, the next question is which spin Hamiltonian(s) imply that order, if we admit interactions J_2 to second neighbors or J_n to further neighbors. The starting point for understanding ordered states is always the classical ground state(s). If the spins sit on a *Bravais* lattice (e.g. face-centered cubic), the solution is trivial due to a rigorous recipe, called the "Luttinger-Tisza" (LT) method (see Sec. II A below): the spins adopt (at most) a simple spiral – a *coplanar* state, meaning all spins point in the same plane of spin space [1, 2]. But if the spins form a lattice with a basis (more than one site per primitive cell), – e.g. kagomé, diamond, pyrochlore, or half-garnet lattices – no mechanical recipe is known to discover the ground state. In these more complicated lattices, magnetic frustration (competing interactions) often induces complicated spin arrangements.

Our aim has been to find a recipe for general lattices (albeit neither exhaustive nor rigorous) to discover the ground state spin pattern corresponding to a given set of exchange couplings J_i, to neighbors at successive distances. That is obviously a prerequisite for solving the inverse problem (given the ordering patterns found by neutron diffraction, which combination(s) of interactions can explain them?). Furthermore, after the whole phase diagram is mapped out, we can identify the parameter sets leading to exceptionally degenerate or otherwise interesting states, so as to recognize which real or model systems might be close to realizing those special states.

In this work, we focus on a narrower question: which parameter combinations give a *noncoplanar* ground state, which could never happen in a Bravais lattice? We adopt the exchange Hamiltonian (1.1), excluding single-site anisotropies J_i, and Dzyaloshinskii-Moriya couplings, which can trivially give non-coplanar ground states.

We do not count cases where a non-coplanar ground state belongs to a degenerate family of states that also includes coplanar ground states. This happens trivially when two sublattices aren't coupled at all, or nontrivially when the interactions are constrained to cancel. In the latter cases thermal or quantum fluctuations usually break the degeneracy, favoring the collinear or coplanar states [3, 4]. (A small amount of site-dilution or bond disorder can generate a uniform effective Hamiltonian that favors non-coplanar states [3, 5], but here we only consider undisordered systems.)

Motivations for noncoplanarity

There are specific physical motivations to hunt for noncoplanar states. First, they point to possible realizations of *chiral* [6] spin liquids, such as are described within bosonic large-N formalisms (as are hoped to approximate the behavior of frustrated magnets with $s = 1/2$). Such formalisms describe transitions from an ordered state to a quantum-disordered spin liquid; since there is no generic reason for a state to stop being chiral at the same time it loses spin order, a chiral ordered state presumably transitions into a chiral spin liquid. Hence, as a rule of thumb, a chiral spin liquid is feasible if and only if the classical ordered state (on the same lattice) is non-coplanar. [7, 8].

Secondly, spin non-coplanarity in metals (usually induced by an external magnetic field) allows the *anomalous Hall effect* observed in pyrochlore and other magnets. [9–12] This is ascribed to spin-orbit coupling and the Berry phases of hopping electrons (which are zero in the collinear or coplanar case).

Thirdly, the symmetry-breaking of noncoplanar exchange-coupled magnetic states is labeled by an order parameter which is an $O(3)$ matrix, so the order-parameter manifold is disconnected. This permits a novel topological defect: the Z_2 domain wall [13], which is only possible in non-coplanar phases.

Finally, there is current interest in "multiferroic" materials (i.e. those with cross couplings of electric and magnetic polar-

izations). For example, in the canonical multiferroics $RMnO_3$ (where R=rare earth), frustrated exchange interactions induce a coplanar spiral, which in the presence of Dzyaloshinskii-Moriya anisotropic interactions carries an electric polarization with it [14–18]. If these spirals were asymmetric conic spirals, like our second class of ground states, there is generically a net moment along the axis, which serves as a convenient "handle" to externally manipulate the orientation of the ground state (and thus control the multiferroic properties).

A. The octahedral lattice

Our spins sit on a rarely studied lattice we christen the "octahedral lattice", consisting of the medial lattice (bond midpoints) of a simple cubic lattice. thus forming corner-sharing octahedra. Thus, each unit cell has a basis of three sites, forming what we call the x, y, and z sublattices (according to the direction of the bond they sit on). Each cubic vertex is surrounded by an octahedron of six sites, with nearest-neighbor bonds forming its edges; these octahedra share corners, much as triangles or tetrahedra share corners in the well-known kagomé and pyrochlore lattices. (Indeed, although the "checkerboard" lattice was introduced as a two-dimensional version of the pyrochlore lattice [19], the octahedral lattice is the best three-dimensional generalization of the checkerboard lattice.) This lattice was first studied as a frustrated Ising antiferromagnet [20, 21] More recently, it was used as a (simpler/pedagogical) toy model in papers aimed at the "Coulomb phase" of highly constrained spins on a pyrochlore lattice [22, 23]. It is one of the lattices constructed from the root lattices of Lie algebras. [24]

The octahedral sites are Wyckoff positions (and hence candidates for a magnetic lattice) in most cubic space groups, so this is plausible to find in real materials, and a few are known. Most simply, it is realized by the transition metal sites in the Cu_3Au superstructure of the fcc lattice [20] (i.e. all but one of the four simple cubic sublattices). So far, the only example known in which the "Cu" lattice is magnetic seems to be Mn_3Ge which is ferromagnetic [25] Another realization is in metallic perovskites such as Mn_3SnN, though again the known materials are ferromagnetic [26]. It would actually seem quite plausible to find realizations of our models, which mostly have several exchange interactions J_i with competing signs, among metallic alloys: the RKKY interaction, expected between local moments in any metal, oscillates with distance inside a slowly decaying envelope.

The octahedral lattice is closely related to the magnetic lattice found in the (mostly metallic) Ir_3Ge_7 structures, including the strong-electron-interaction superconductor Mo_3Sb_7 [27, 28]. In that lattice, the simple-cubic lattice sites are surrounded by *disjoint* octahedra, i.e. a dimer of *two* magnetic ions decorates each bond of the simple cubic lattice. If this dimer were strongly coupled ferromagnetically, it would be a good approximation to treat it as a single spin, which is exactly the octahedral lattice. Instead, in Mo_3Sb_7 the dimers are antiferromagnetically coupled and, since Mo has spin 1/2, they form singlets [28]. If the spin length were longer, justify-

ing classical treatment, we could convert to the ferromagnetic case simply by inverting the spin directions in every octahedron around an odd site of the cubic lattice, and changing the sign of all bonds coupling even sites with odd sites. Thus, much of the classical phase diagram for the Mo_3Sb_7 lattice is related to that of the octahedral lattice.

In this paper, we mainly consider four kinds of couplings, for separations out to the third neighbors: J_1 for $\langle 1/2, 1/2, 0 \rangle$, J_2 or J_2' for $\langle 1, 0, 0 \rangle$, J_3 for $\langle 1, 1/2, 1/2 \rangle$. Notice that couplings with the same displacement need not be equivalent by symmetry, since the site symmetry is just fourfold, less than cubic. (Our naming convention is to use the prime for the separation which requires more first-neighbor steps to traverse.) We also (less extensively) consider interactions J_4 or J_4' for $\langle 1, 1, 0 \rangle$. To organize our exploration of this parameter space, in analytic calculations we shall often assume $J_3, J_4, J_4' \ll J_1, J_2, J_2'$ (that suffices to give examples of most of the classes we found of noncoplanar ground states).

B. Outline of paper and preview of results

We begin (Sec. II) by developing the techniques and concepts necessary to find the phase diagram as a function of the J_{ij}'s and to discover *non-coplanar* ground states. We found ground states using three methods. The first (Sec. II A was Fourier analysis, known as the "Luttinger-Tisza" method, which can give a lower bound on the energy, but may not give a full picture of the ground state. The second (Sec. II B is an iterative minimization algorithm, which numerically converges to a ground state; we introduce several diagnostic tools for understanding the spin patterns produced by iterative minimization. The third method (Sec. II C) is the variational optimization of idealized patterns displayed by iterative minimization.

We then turn to our results, beginning with descriptions of the several classes of magnetic state we found for the octahedral lattice: various coplanar states (Sec. III), the noncoplanar, commensurate "cuboctahedral" spin states (Sec. IV), and a more generic group of noncoplanar, incommensurate "conic spirals" (Sec. V); in these the lattice breaks up into layers of spins with the same directions, each layer being rotated around the same (spin-space) axis relative to the layer below. Particularly noteworthy was a "double-twist" state we encountered, which is something like a conic spiral which also has a complex modulation in the transverse directions (Sec. VI). The plain stacked structures can be studied by mapping to one-dimensional ("chain") lattices, also with couplings to many neighbors, as worked through in Sec. V B.

From this we go on (Sec. VII) to quickly survey the phase diagrams we found, first for the cuboctahedral lattice, and then for the chain lattice (when treated as a lattice in its own right). In the conclusion, Sec. VIII, we reflect on what our results might suggest for other frustrated lattices, such as the pyrochlore.

II. METHODS AND FRAMEWORK

We employed several approaches to discover and understand ground states, for each given set of interactions (these are developed rest of this section – except for the use of mappings, which we explain in Sec. V, where it becomes natural to employ this technique).

(a) . A Fourier analysis of the Hamiltonian (1.1) as a quadratic form with coefficients J_{ij}, the so-called "Luttinger-Tisza" method outlined in Sec. II A.

(b) . Iterative minimization, our main "exploratory" technique. Starting from a random initial condition, we successively adjusted randomly chosen spins so as to reduce the energy. (Sec. II B). We then analyzed each resulting pattern with various diagnostics, as described in Sec. II B, and tagged the non-coplanar ones for further investigation.

(c) . Variational optimization of the iterative minimization ground state. Finding a closed-form for the ground state introduces a number of free parameters (the most obvious being a wave-vector). By allowing these parameters to vary from the values found with iterative minimization, we find a new, more rigorous, ground state.

(d) . Mapping the (three-dimensional) problem to a similar problem in a one-dimensional "chain" lattice with a basis of two sites. This is valid when the optimal (three dimensional) spin configuration is a stacking of layers, which we judged based on the results from approaches (a) and (b). The states on this simplified chain lattice may be found using approaches (a) and (b), or analytically solved after parametrizing the state with a set of variational parameters.

A. Spin states and Luttinger-Tisza modes

The general theory of spin arrangements is reviewed in Refs. 2 and 29. The most fruitful approach to finding the ground states of the Hamiltonian (1.1) is to treat it as a quadratic form rewriting (1.1) as

$$\mathcal{H} = -\sum_{\mathbf{k}} \sum_{\alpha,\beta=1}^{m} \tilde{J}_{\alpha\beta}(\mathbf{k})\tilde{\mathbf{s}}_{\alpha}(-\mathbf{k}) \cdot \tilde{\mathbf{s}}_{\beta}(\mathbf{k}), \qquad (2.1)$$

where α and β are sublattice indices; the explicit formulas for the cuboctahedral lattice case are given in Appendix A 1, Eq. (A1). Then we diagonalize this matrix, obtaining

$$\mathcal{H} = -\sum_{\mathbf{k}} \sum_{\nu=1}^{m} \tilde{J}(\mathbf{k}\nu)|\tilde{\mathbf{s}}(\mathbf{k}\nu)|^2. \qquad (2.2)$$

Here $m = 3$ is the number of sites per primitive cell, and ν is a band index; thus $\{\tilde{J}(\mathbf{k}\nu)\}$ are the eigenvalues of J_{ij} as an $mN \times mN$ matrix, with N being the number of cells (to be taken to infinity), and the wavevector $\mathbf{k}$ runs over the Brillouin zone. [In the Bravais lattice case, $m = 1$, the eigenvalue $\tilde{J}(\mathbf{k})$ is simply the Fourier transform of $J(\mathbf{r})$; for $m > 1$.] Also, $\tilde{\mathbf{s}}(\mathbf{k}\nu)$ (complex-valued 3-vector) is the projection of the spin configuration onto the corresponding normalized eigenmode, $N^{-1/2}v_{\nu s}\exp i(\mathbf{k} \cdot \mathbf{r})$. We shall call these the "Luttinger-Tisza" (LT) eigenvalues and modes [2, 30, 31]; a mode with the most negative $\tilde{J}(\mathbf{k}\nu)$ is called an "optimal" mode, and its wavevector is called $\{\mathbf{Q}_{\mathrm{LT}}\}$.

The ideal case is that we can build a spin state satisfying two conditions

> *Condition (1)* $\{\mathbf{s}_i\}$ are entirely linear combinations of optimal LT modes

> *Condition (2)* $|\mathbf{s}_i|^2 = 1$ everywhere (unit length constraint)

If both conditions are satisfied, these *must* be ground states, and all ground states *must* be of this form.

In the case of a Bravais lattice ($m = 1$), the LT modes are just plane waves $e^{i\mathbf{k}\cdot\mathbf{r}}$, and one can always construct a *planar* spiral configuration [1], $\mathbf{s}(\mathbf{r}) = \cos(\mathbf{Q}_{\mathrm{LT}} \cdot \mathbf{r})\hat{\mathbf{B}} + \sin(\mathbf{Q}_{\mathrm{LT}} \cdot \mathbf{r})\hat{\mathbf{C}}$, where $\hat{\mathbf{B}}$ and $\hat{\mathbf{C}}$ are orthogonal unit vectors, and the spatial dependence consists only of optimal modes [2]. In the simplest cases, $\mathbf{Q}_{\mathrm{LT}}$ is at high symmetry points on Brillouin zone corners, and one can construct a combination of optimal modes which is ± 1 on all sites, which defines a *collinear* ground state, as in the phase diagrams in Ref. 32.

Thus, non-Bravais lattices are *necessary* in order to get non-coplanar states. (But not sufficient: it appears that, on non-Bravais lattices with high symmetry, the commonest ground states are still collinear or coplanar.) In lattices-with-a-basis, however, the LT eigenmodes have different amplitudes on different sites within the unit cell, and it is not generally possible to make any three-component linear combination of the best modes that satisfies the unit-length constraint. (There is an exception for lattices in which the neighbors-of-neighbors are all second neighbors, such as the diamond [33] or honeycomb [34] lattices.)

A "generalized" L-T method for non-Bravais lattices was introduced by Ref. 35 (see also Ref. 36) and applied to spinels with both A and B sites magnetic [2, 31]. However, this method involves site-dependent variational parameters, so one must already understand the pattern of the ground state in order to make it into a finite problem; in practice, this method appears quite similar to our method (Sec. V and A 2) of projecting a layered structure to a one-dimensional chain.

Although the LT optimal modes (usually) give the *exact* ground states in the cases we focus on, we believe the exact ground state is frequently built mainly from almost-optimal modes; that is, although a linear combination of optimum LT modes violates the unit-spin constraint, with a small distortion it may satisfy the constraint and be the ground state. (That distortion necessitates admixing other modes but with small amplitudes, since they carry a large energy penalty, according to (2.2).) In particular, we anticipate that (for incommensurate orderings) the true ordering wavevector lies in the same symmetry direction as the LT wavevector; and that the phase diagram for optimum LT wavevectors mostly has the same

topology as the actual phase diagram for ground states. Thus the LT modes can serve as a "map" for navigating the parameter space of $\{J_i\}$ and for understanding the ground state spin configurations.

An important caveat is that almost all $\mathbf{Q}$ vectors have symmetry-related degeneracies, and the LT analysis is silent on how these modes are to be combined with different spin directions, so the specification of the actual spin configuration is incomplete. (An example is the "double-twist" state, of Sec. VI.) As a corollary, a single phase domain on the LT mode phase diagram might be subdivided into several phases in the spin-configuration phase diagram, that represent different ways of taking linear combinations of the same LT modes. This cannot be detected at the LT level.

One immediate insight is afforded by considering the LT phase diagram. Short-range couplings have Fourier transforms $\tilde{J}_{\alpha\beta}(\mathbf{k})$ in (2.1) that vary slowly in reciprocal space. Such functions typically possess extrema at high-symmetry points in the Brillouin zone; the same is probably true for the optimum *eigenvalues* and their wavevectors $\mathbf{Q}_{\mathrm{LT}}$. That corresponds to simple, commensurate ordering in real space. In order to get the optimal LT mode (and presumably the actual ordering) to be incommensurate, or to possibly stabilize states with stacking directions other than (100), one needs to include more distant neighbor couplings.

In practice, we never used LT to directly discover the ground state spin configuration; its value is to quickly prove a given state is a ground state. But the LT viewpoint did inform the Fourier-transform diagnostic we used in analyzing the outputs of iterative relaxation (Sec. II B. Furthermore, when we operated in the "designer" mode (seeking the couplings that stabilize a specified state) we used the LT modes as a guide or clue: namely, we found the $\{J_i\}$ that made the ordering wavevector $\mathbf{Q}$ of our target state to be the optimal $\mathbf{Q}_{\mathrm{LT}}$, which is easier than making $\mathbf{Q}$ be the ordering wavevector of the actual ground state.

B. Iterative minimization

Our prime tool for exploration was iterative minimization starting from a random initial condition. Random spins are selected in turn and adjusted (one at a time) so as to minimize the energy, by aligning with the local field of their neighbors, till the configuration converged on a local minimum of the Hamiltonian. [37]. (Our criterion was that the energy change in one sweep over the lattice was less than a chosen tolerance, typically 10^{-9}).

It might be worried that such an algorithm gets stuck in metastable states, unrepresentative of the ground state; such "glassy" behavior is indeed expected in the case of Ising (or otherwise discrete) spins, or in *randomly* frustrated systems such as spin glasses. However, vector spins typically have sufficient freedom to get close to the true ground state [38, 39]. The typical ways they deviated from the ground state are just long-wavelength wandering ("spin waves") or twists of the spin directions.

The only problem with the dynamics is that our algorithm is a variant of "steepest descent", one of the slowest of relaxation algorithms. such deviation modes are indeed slow relaxing For this kind of (local) dynamics, the relaxation rate of a long-wavelength spin wave at wavevector $\mathbf{q}$ is proportional to $|\mathbf{q}|^2$, i.e. $1/L^2$ for the slowest mode in a system of side L. (In future applications, some version of conjugate gradient should be applied to give a faster convergence, or – if there is a problem is finding the right valley of the energy function – one might adapt Elser's "difference map" approach to global optimization [40].)

For initial explorations, we usually used very small cubic simulation boxes of L^3 cells ($L = 3, 4,$ or 5). For each set of $\{J_{ij}\}$ tested, we tried both periodic and antiperiodic boundary conditions, as well as even or odd L. Usually one of those four cases accomodates an approximation of the infinite system ground state, though of course any incommensurate state must adjust either by twisting to shift the ordering wavevector to the nearest allowed value, or else (as we observed) via the formation of wall defects. We tried to distinguish the ground states which were "genuine" in that a similar state would remain stable in the thermodynamic limit. In particular, out of the four standard systems we tried (even/odd system size, periodic/antiperiodic BC's), a "genuine" state should be the one with lowest energy.

For a large portion of the parameter space, the ground states were planar spirals, essentially no different from the solutions guaranteed in the Bravais lattice case. Many of the noncoplanar configurations found were "non-genuine" artifacts of finite size when the periodic (or antiperiodic) boundary conditions and dimension L were incompatible with the natural periodicity of the true ground state. One might expect the wrong boundary condition to simply impose a twist by π/L per layer on the true ground state, but instead the observed distortion of the spin texture was sometimes of the natural periodicity of the ground state, a "buckling" occurred; that is, the configuration consists of finite domains similar to the true ground state, separated by soliton-like domain walls.

The greatest difficulty in our procedure was not obtaining an approximation of the ground state, or even deciding whether it was genuine. Rather, it was grasping what the obtained pattern is, and how to idealize it to a periodic (or quasiperiodic) true ground state of the infinite system. We were aided by the following three diagnostics.

1. Diagnostic: Fourier transform:

Configurations obtained by iterative minimization were Fourier transformed and the norms of each Fourier component $\sum_s |\tilde{\mathbf{s}}(\mathbf{k}, s)|^2$ were summed (combining the sublattices) [41]. This suffices to identify the state when it is a relatively simple antiferromagnetic pattern, or an incommensurate state described as a layer stacking. In any case, the results can be compared to the LT mode calculation to see if the found state achieves the LT bound.
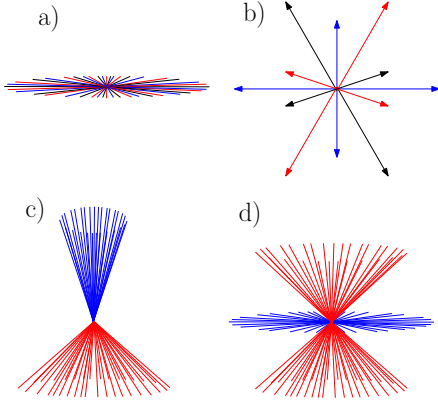
FIG. 1: (COLOR ONLINE). Common-origin plots for four kinds of spin ground states on the octahedral lattice, appearing for different choices of the exchange interactions $\{J_i\}$. (a). planar spiral (b). cuboctahedral state (c). asymmetric conic spiral (d). alternating conic spiral.

2. Diagnostic: common-origin plot:

The simplest visual diagnostic of a state is the "common-origin plot", in which each spin's orientation is represented as a point on the unit sphere. For example, an incommensurate coplanar spiral state would appear as a single great circle on the common-origin plot (see Fig. 1).

A drawback of the common-origin plot is the lack of information on the spatial relation of the spins. (For example, a "cone" might appear consisting of closely spaced spin directions, but these might belong to widely spaced sites.) Furthermore, this diagnostic is quite fragile in configurations where a domain wall or other defect has been quenched in.

In the case of one-dimensional chains (see Sec. V B), we may instead use the "end-to-end" spin plot, where the tail of each spin vector is on the head of the previous spin vector. The advantage is that (i) images are not so obscured by overlaying of different vectors, and (ii) spatial information is captured, in particular defects where the state has "buckled". [42]

In tandem with the common-origin plot, an algorithm was used that found groups of spins with (nearly) identical spin directions, within a chosen tolerance (typically, a dot product greater than 0.99). For commensurate patterns comprising a finite set of spin directions, this allowed the magnetic unit cell and spin configuration to be read off, but it was useless for incommensurate states, in which no spin direction exactly repeats.

3. Diagnostic: Spin moment-of-inertia tensor

We computed the 3×3 tensor

$$M_{ij} \equiv \frac{1}{mN} \sum_{\alpha,r} (\mathbf{s}_i(\vec{r}))_\alpha (\mathbf{s}_j(\vec{r}))_\alpha \qquad (2.3)$$

(notice $\mathrm{Tr}(\mathbf{M}) = 1$) and diagonalized it. We recognize coplanar or non-coplanar spin states as those where $\mathbf{M}$ has two or three nonzero eigenvalues, respectively. (Rotating the spin configuration so the principal directions of $\mathbf{M}$ are the coordinate axes usually manifests the spin configuration's symmetries.)

C. Variational Optimization

Through the diagnostic techniques described in the previous subsections, it is normally straightforward to parameterize the spins in the ground as $\mathbf{s}(\mathbf{r}, \{\alpha\})$, i.e. as a function of position and some arbitrary set of parameters, $\{\alpha\}$. The exact values of these parameters can (formally) be calculated from optimizing $\mathcal{H}(\mathbf{s}(\mathbf{r}, \{\alpha\}), \{J\})$. One major advantage of relying upon this method is that it reduces the effect of numerical artifacts from iterative minimization. For example, we no longer enforce an arbitrary periodicity upon the LT wavevector.

D. Conceptual framework for bridging states

This subsection is not about a technique, but a classification of two ways that ground states may be related to each other, and thus of two kinds of phase boundaries in the phase diagrams (Sec. VII and Appendix A). We call these two concepts "encompassing states" and "families of degenerate states".

1. Encompassed states

We call a ground state "encompassed" if it is a special case of another, more general state. For example, a ferromagnet is encompassed by a helimagnet, since letting the helimagnetic angle go to zero produces a ferromagnet. "More general" means there is a continuous family of states such that each particular combination of couplings J_i's completely determines a particular member of that family. Moreover, the (more general) encompassing state necessarily spans at least one more dimension of spin space, so if the encompassed state is coplanar, the encompassing one is non-coplanar. However, while every encompassing state is more general than the state it encompasses, not every more general state will encompass a particular ground state. For example, the asymmetric conic is more general than the splayed ferromagnet (both of these states are defined in Sec. V), but it does not encompass the splayed ferromagnet; there is, however, a third class that encompasses both these classes.

2. Degenerate states

By contrast, "degenerate states" means that for certain combinations of J_i's, there is a continuous family of exactly degenerate ground states. Most commonly, this is the result of *decoupling* between sublattices of spins, meaning one can apply a global rotation limited to just one of the sublattices while remaining in the degenerate manifold. This can come

about in two ways. The trivial way is when all J_i's that couple those sublattices vanish. The more interesting way is when the couplings are nonzero, but cancel generically in all the ground states; the simplest example of this kind is the J_1–J_2 antiferromagnet on the square [3] or bcc [4] lattice, in the J_2-dominated regime in which each of the even and odd sublattices realizes plain Néel order. Apart from decoupling, degenerate manifolds are also sometimes realized by simultaneous rotations involving all sublattices with some mutual constraint (e.g. in the nearest-neighbor kagomé lattice, the constraint that the spins add to zero in every triangle).

Independent of the categories mentioned, these degenerate families may either be *simply degenerate*, meaning the ground state manifold is labeled by a finite number of parameters – one nontrivial angle in the case of the J_1–J_2 antiferromagnet – – or else *highly degenerate*, meaning the number of parameters scales with size as $O(L^n)$ with $n > 0$. An example with trivially decoupled, highly degenerate ground states is a layered lattice with vanishing interlayer couplings, so the number of free parameters scales as $O(L)$; the $J = 1$ kagomé antiferromagnet is a mutally constrained, highly degenerate case with $O(L^2)$ parameters, i.e. extensively many.

Both the simply and highly degenerate families also have clear signatures in reciprocal space. In the simple case, the optimal wavevectors are discrete and related by symmetry, e.g. the J_1–J_2 square lattice antiferromagnet has $\mathbf{Q}_{\mathrm{LT}} = (1/2, 0)$ or $(0, 1/2)$; in this case, the degeneracy lies in the freedom to mix these degenerate LT eigenmodes with different coefficients, not from the presence of extended (one-, two-, or even three-dimensional) surfaces in the Brillouin zone. By contrast, in the highly degenerate scenario, typically holding for special combinations of couplings, the LT optimum wavefectors occur not just at isolated $\mathbf{Q}_{\mathrm{LT}}$ in the Brillouin zone, but on extended (one-, two-, or even three-dimensional) surfaces, i.e. one has degenerate eigenmodes of the LT matrix that are not symmetry-equivalent. The rhombohedral lattice with J_1, J_2, and J_3 has a degenerate one-parameter family of wavevectors corresponding to different coplanar spirals [43]. The three-dimensional pyrochlore lattice with only nearest-neighbor (J_1) couplings is a well-known example of the highly degenerate scenario, requiring extensive number of parameters. In that case, the minimum LT eigenvalue is uniform throughout the Brillouin zone [44] (a so-called "flat band").

3. Encompassed and degenerate states as bridges in phase diagram

What encompassing states and families of degenerate states have in common is to serve as bridges between simple states.

In the "encompassing" case, the encompassing state is typically stable in a domain of parameter space of nonzero measure. When one adjacent phase in a phase diagram is encompassed by the other, they are necessarily related (in our $T = 0$ phase diagram) by a continuous transition, usually involving a symmetry breaking.

In contrast, degenerate families are (frequently) confined

to phase boundaries. Even when they occupy a finite area in a slice of parameter space (e.g. the (J_1, J_2) plane when all other couplings are zero), turning on additional couplings can remove the degeneracy.

A corollary is that the naive classification of continuous or first-order phase transitions does not work. Consider two phases separated by a phase boundary on which a degenerate family is stable. Each of the two phases (or the limit of either as the boundary is approached) is a special case from the degenerate family. Since the limits taken from the opposite directions are different, it appears at first as an abrupt transition. On the other hand, it is possible to take the system continuously from one phase to the other if we pause the parameter variation when we hit the phase boundary, and follow a path through the degenerate manifold from one of the limiting states to the other one.

Furthermore, turning on additional parameters generically destroys the degeneracy. That converts the degenerate family into an encompassing family, and the single phase boundary into two continuous ones. Specifically, starting in one of the main phases, we cross a small strip of phase diagram in which the configuration evolves (determined by the parameter combination) from one of the limiting states to the other one, and then enter the other of the main phases. Thus, the "encompassed" kind of transition is distinct from either a first-order transition (between two unrelated states) or an ordinary continuous one, and will be indicated on phase diagrams with a distinct kind of line.

E. Cluster analysis: two degenerate ground states

The "cluster" method is a rigorous analytic approach to ground states, alternative to the LT mode approach. [45], which depends on decomposing the Hamiltonian into terms for (usually overlapping) clusters, and finding the ground states for one cluster. If these ground states can be patched together so as to agree where they overlap, the resulting global state must be a ground state and all ground states must be decomposable in this fashion. In this way we can characterize the degenerate states appearing for two special combinations of J_i's.

1. Antiferromagnetic J_1 only

In this case, the cluster is a triangle (one face of an octahedron, including one site each from the x, y, and z sublattices). The ground state of such a triangle is the usual $120°$ arrangement of spins. If all such triangles are to be satisfied, then wherever two of them share an edge, the respective unshared spins are forced to have identical directions – in the present case, spins on opposite corners of the octahedron. Thus, a line of x sublattice spins in the x direction (or similarly of the other sublattices in their directions) is constrained to be the same.

This high degeneracy is not limited to the single point in parameter space $J_1 < 0$. If we turn on J_2, which couples the

nearest neighbors aling those lines of spins, the same configurations remain the ground state until J_2 is negative and its magnitude sufficiently large compared to $|J_1|$; less obviously, the same thing is true for $J_3 = J_4$, varied together.

This allows two different kinds of highly degenerate state:

(a) One sublattice (say x) has $\mathbf{s}_i = +\hat{\mathbf{A}}$ along every line. Within the other sublattices, each yz plane has an independent rotation about the $\hat{\mathbf{A}}$ axis. Thus the spin directions are

$$\mathbf{s}_i = -\frac{1}{2}\hat{\mathbf{A}} \pm \frac{\sqrt{3}}{2}\hat{\mathbf{B}}(x), \qquad (2.4)$$

where $\hat{\mathbf{B}}$ is a different unit vector in each plane, and we take the $+$ or $-$ sign in the y or z sublattice, respectively.

The common-origin plot for this state looks superficially like a conic spiral, the cone being formed by the y and z spin directions. In reality, whereas an incommensurate spiral gives a uniform weight along the spiral in the common-origin plot, this state gives a random distribution which approaches uniformity only in the limit of a very large system.

(b). For a second family of (discretely) degenerate states, we choose

$$\mathbf{s}(n_1 + 1/2, n_2, n_3) = \frac{1}{\sqrt{2}}[0, f_2(n_2), -f_3(n_3)]; \quad (2.5\text{a})$$

$$\mathbf{s}(n_1, n_2 + 1/2, n_3) = \frac{1}{\sqrt{2}}[-f_1(n_1), 0, f_3(n_3)]; \quad (2.5\text{b})$$

$$\mathbf{s}(n_1, n_2, n_3 + 1/2) = \frac{1}{\sqrt{2}}[f_1(n_1), -f_2(n_2), 0]. \quad (2.5\text{c})$$

where $f_i(n_i) = \pm 1$ are arbitrary. Notice that (2.5c) uses (a subset of) the cuboctahedral directions. Typically, in a sufficiently large system, all those directions are used nearly equally; the common-origin plot would show a cuboctahedron. However, the spins do not have a regular pattern in space since (2.5c) is random, with a discrete degeneracy $O(L)$ in a system of L^3 cells. The states (2.5c) represent a degenerate family of states, as formulated in Sec. II D: the optimum LT eigenvalues are found at *all* wavevectors $\mathbf{Q}$ lying on the (100) axes.

We are *not* interested in the high degeneracy for its own sake; its significance is that various kinds of ordered states can be selected out of it, by turning on additional couplings (even infinitesimally). Thus, the high-degeneracy parameter combinations will be corners of phase domains in the phase diagram.

2. Antiferromagnetic J_1 and J_2

Let $\mathbf{L}_\alpha$ be the net spin of the octahedron centered on α.

$$\mathbf{L}_\alpha \equiv \sum_{i \in \alpha} \mathbf{s}_i \qquad (2.6)$$

where α is a cubic lattice vertex and $i \in \alpha$ means site i is on one of the six bonds from α, Consider a Hamiltonian written as

$$\mathcal{H} = \frac{J}{2}\sum_\alpha |\mathbf{L}_\alpha|^2. \qquad (2.7)$$

On the one hand, expanding the square shows this is simply the antiferromagnet with $J_1 = J_2 = J$. On the other hand, it is obvious from (2.7) that any configuration with a net (classical) spin of zero on every octahedron is a ground state. This is another example of a degenerate ground state family (Sec. II D); in this case the continuous degeneracy is macroscopic. This Hamiltonian is constructed in exactly the same way as those of well-known highly frustrated lattices (kagomé, checkerboard, half-garnet, pyrochlore) that have similar ground state degeneracies.

III. COPLANAR STATES

Several different collinear or coplanar ground states can be stabilized within the octahedral lattice, only one of which requires couplings beyond J_2. We will describe them from the smallest to the largest magnet unit cells. The most elementary of these is the ferromagnetic state, in which all spins are aligned in the same direction, and which obviously requires predominantly positive couplings. This state is composed of a (0,0,0) LT mode with equal amplitudes on every sublattice (so the normalization condition is already satisfied).

There is also the "three-sublattice 120° antiferromagnetic state", whose unit cell is the primitive cell. Each of the three sublattices has a uniform direction; the net inter-sublattice couplings are antiferromagnetic, so (as in the ground state of a single antiferromagnetic triangle) the respective spin directions are 120° apart and coplanar. Thus this state, too, is characterized by ordering wavevector $\mathbf{Q} = (0, 0, 0)$, but not the same LT mode as the ferromagnetic state. Instead, this one is from the two degenerate modes at $\mathbf{Q} = (0, 0, 0)$ that are orthogonal to the uniform mode. (Any combination of these modes has unequal magnitude on the different sublattices, which is why *both* modes need to be present in the spin state, combined with different spin directions.) This state is a special case of the highly degenerate ground states found when only $J_1 < 0$ (Sec. II E 1).

The next group of coplanar states are the $\mathbf{Q} \neq 0$ antiferromagnetic states, of which there are three kinds, characterized by having ordering wavevectors of type (0,0,1/2), (0,1/2,1/2), or (1/2,1/2,1/2). Each of these states is antiferromagnetic overall within every sublattice; the sublattices decouple, since any inter-sublattice interaction couples a spin in one sublattice to equal numbers of spins pointing in opposite directions in the other sublattice. These are LT states; in the (0,0,1/2) and (0,1/2,1/2) cases, the LT mode used is nonzero on only one sublattice, and a different one of the three symmetry-related wavevectors is used for each sublattice (the one with the same distinguished direction). e.g. the x sublattice uses (1/2,0,0) or (0,1/2,1/2) modes. Notice that in these two cases, the spins repeat ferromagnetically along some directions (within a sublattice); this is a consequence of the anisotropy of the intra-sublattice couplings. Qualitatively, these states are stable when J_2 is different from J_2'. All of these states can be realized with collinear spins.

Lastly, the octahedral lattice admits helimagnetic states. These states require at least J_3 couplings to become stabilized.

The helimagnetic states must be composed entirely out of (q, q, q) modes. This is because any other wave-vector would break the symmetry between the sublattices. More precisely, helimagnetic states are generically a function of one variable, $\vec{k} \cdot \vec{r}$, and are therefore equivalent to a one-dimensional system. It will therefore be amenable to stacking vector analysis, developed in V. But using stacking vectors to transform the octahedral lattice to a one-dimensional chain will necessarily produce a non-Bravais lattice unless the stacking vector (111) (or a permutation of sign). And any helimagnetic mode in the one-dimensional non-Bravais lattice will break normalization in the octahedral lattice, since some spin directions would be represented more than others (this will be allowable for conics because they mix multiple modes, but helimagnets are explictly single mode). Therefore, the only allowable stacking vector (and by implication, wave-vector) is (111).

IV. CUBOCTAHEDRAL STATES

The octahedral lattice possesses two kinds of "cuboctahedral" state, stable in different domains of parameter space, for which the common-origin plot takes the form of a cuboctahedron, i.e. twelve spin directions of the form $(1, 1, 0)/\sqrt{2}$ and its permutations [Fig. 1(b)]. The magnetic unit cell is $2 \times 2 \times 2$ for both of these true cuboctahedral states (spuriously cuboctahedral states were remarked in Sec. II E 1). They differ in that the angles between neighboring spins (which are in different sublattices) is $60°$ in one kind of cuboctahedral state but is $120°$ in the other kind.

As worked through in this section, the cuboctahedral states can be understood from any of three approaches:

(a) Cluster construction: the Hamiltonian can be decomposed into a sum of terms, each for an octahedron; we can patch together the ground states of the respective octahedra to obtain a ground state of the whole lattice. (For $60°$ cuboctahedral only.)

(b) Degenerate perturbation theory: two special sets of couplings give degenerate families of ground states, out of which a small additional coupling can select the cuboctahedral state. (For $120°$ cuboctahedral only.)

(c) The Luttinger-Tisza framework of Sec. II A. (For both kinds of cuboctahedral state.)

The $120°$ cuboctahedral state is a subset of the J_1–only antiferromagnetic ($J_1 < 0$) ground states described above (Sec. II E 1). Thus, this state is stabilized even in the limit as J_2 (or other distant couplings) become arbitrarily small. It is the only non-coplanar state we found that does not require any couplings beyond J_2 and J_2'.

A. Lattice as union of cuboctahedral cage clusters

The first cuboctahedral state noticed was in the J_1–J_2 magnet on the kagome lattice [46, 47], with J_1 ferromagnetic and J_2 antiferromagnetic. There is a range of ratios J_2/J_1 in which the magnetic unit cell on the kagome lattice is 2×2. Taking that cell as given, the possible ground states are those of the twelve-site cluster made by giving periodic boundary conditions to one unit cell – a cluster which is topologically equivalent to a single cuboctahedron (even when couplings to any distance are taken into account), and hence include the cuboctahedral state.

Turning to the present case of the octahedral lattice, in fact this is a union of cuboctahedral cages surrounding cube centers, complementary to the octahedral clusters surrounding the cube vertices. We can apply the "cluster" construction (see Sec. II E) to these cages by representing its lattice Hamiltonian as a sum of cuboctahedron Hamiltonians, with $j_1 = J_1/2$, $j_2 = J_2/2$, $j_2 = J_2'/2$, and $j_4 = J_4/2$ (J_1, J_2, J_2' and J_4 are shared by two cuboctahedra); also $j_3 = J_3$ and $j_4' = J_4'$.

Consider for a moment the ground state of 12 spins placed on an isolated cuboctahedron, [48] with couplings j_1, j_2, j_3, and j_4. Now, it is well known that, on a chain (i.e. a discretized circle), $j_1 > 0$ and (small) $j_2 < 0$ give a gradual, coplanar spin spiral; on a circle with the right number of sites the spin directions point radial to that circle. Roughly speaking, the three-dimensional analog of this happens on a cuboctahedron, which is a discretized sphere: if j_1 is ferromagnetic and one of the more distant couplings is antiferromagnetic, the spin ground state is a direct image of the center-to-vertex vector in the cuboctahedron (modulo a global $O(3)$ rotation of the spins). This notion only works for the $60°$ kind of cuboctahedral, occurring for $J_1 > 0$, in which the nearest neighbors are (relatively) close to being parallel.

To build a global state in which every cuboctahedron has the cuboctahedral spin configuration, the difficult part is just to make the spins agree where they are shared between cuboctahedra: that is achieved by applying mirror operations in alternate layers of cuboctahedra, such that e.g. the s_i^x components are multiplied by $(-1)^{x/a}$.

B. As special case of J_1-only antiferromagnet

When we have only $J_1 < 0$ couplings, the ground state is a degenerate state with $120°$ angles between nearest neighbors, as written in Eq. (2.5c) of Sec. II E 1. In that degenerate state of Sec. II E 1 the spins take (some of or all of) the cuboctahedral directions, but do not have a genuine cubic spin symmetry. As soon as an arbitrarily small antiferromagnetic J_2 is added as a perturbation, a subset of these states is selected, which is the $120°$ kind of cuboctahedral state. In the notation of (2.5c), this true 120∘ cuboctahedral state takes the following form:

$$\mathbf{s}(n_1 + \tfrac{1}{2}, n_2, n_3) = \frac{1}{\sqrt{2}}[0, (-1)^{n_2}, (-1)^{n_3}]; \quad (4.1a)$$

$$\mathbf{s}(n_1, n_2 + \tfrac{1}{2}, n_3) = \frac{1}{\sqrt{2}}[(-1)^{n_1}, 0, \pm(-1)^{n_3}]; (4.1b)$$

$$\mathbf{s}(n_1, n_2, n_3 + \tfrac{1}{2}) = \pm\frac{1}{\sqrt{2}}[(-1)^{n_1}, (-1)^{n_2}, 0]. (4.1c)$$

where $+$ corresponds to the $120°$ state and $-$ to the $60°$.

C. Luttinger-Tisza approach to cuboctahedral states

Alternatively, both cuboctahedral states can be understood within the LT framework. For certain domains of parameter values, the optimal LT modes have wavevectors $\mathbf{Q}_{LT}$ of $\{1/2, 0, 0\}$ type. It can be worked out that for e.g. $\mathbf{Q}_{LT} = (1/2, 0, 0)$, one eigenmode has amplitudes $(1, 0, 0)$ on sublattices (x, y, z), i.e. its support is only on the x sublattice. Each of the other two eigenmodes has its support equally on the y and z sublattices, the amplitudes being $(0, 1, \pm1)$. When the first eigenmode is optimal, we get the decoupled $(1/2, 0, 0)$ antiferromagnet already described in Sec. III; when either of the two-sublattice eigenmodes is stable, a cuboctahedral states is found.

It is obviously impossible to satisfy normalization in a spin state using just one of the two-sublattice modes, since its amplitude vanishes on the third sublattice. To build a normalized ground state, it is necessary and sufficient to form a linear combination using all three of the symmetry-related $\mathbf{Q}_{LT}$ wavevectors, associating each with a different orthogonal spin component. Thus the spin directions are $(1, 1, 0)/\sqrt{2}$, with all possible permutations and sign changes, as we already saw in Eq. (4.1). These states could be called a commensurate triple-Q state. The eigenmode with amplitudes of form $(0, 1, 1)$ gives the $60°$ cuboctahedral whereas the one of form $(0, 1, -1)$ gives the $120°$ cuboctahedral state.

1. Absence of (1/2, 1/2, 0) Cuboctahedral State

From the LT viewpoint, one would naively expect to construct similar noncoplanar cuboctahedral states of cubic symmetry using $\mathbf{Q}_{LT}$ of (1/2,1/2,0): why are they absent? After all, the $\{1/2, 1/2, 0\}$ type wavevectors are threefold degenerate, just like the (1/2,0,0) wavevectors from which the cuboctahedral states are built, and it is straightforward to follow the analogy of those states to construct a (1/2, 1/2,0) cuboctahedral (just allotting each mode one of the three cartesian directions in spin space). Furthermore, if we include J_4 and J_4' couplings in the Hamiltonian, there is a certain region of parameter space in which $\mathbf{Q}_{LT} = (1/2, 1/2, 0)$ can indeed be optimal, with the optimal LT eigenmodes being orthogonal to the eigenmodes that make up the $(1/2, 1/2, 0)$ type antiferromagnetic state. Hence in that region, the putative $(1/2, 1/2, 0)$, cuboctahedral state really is a ground state.

But closer examination of the LT matrix for $\mathbf{k} = (1/2, 1/2, 0)$ shows that neither the cuboctahedral state, nor any noncollinear state, is *forced*. At this high symmetry point in the Brillouin zone, all intersublattice contributions to the LT matrix $\tilde{J}_{\alpha\beta}(\mathbf{k})$ [see Eq. (2.1)] cancel. That means the $(\tilde{J}_{\alpha\beta})$ is a diagonal matrix. Its eigenvalues are $-J_2 + 2J_2' - 4J_4 - 2J_4'$ for the mode of the (1/2,1/2,0) antiferromagnet, plus two degenerate eigenvalues $J_2 + 2J_4'$ for the modes of interest here.

Furthermore, the fact that only J_2 and J_4' enter the formula indicates that all other couplings cancel out. Not only are spins of different sublattices decoupled, but each sublattice decouples into two interpenetrating (and unfrustrated) tetragonal lattices . (The latter decoupling is reminiscent of the decoupling of the J_2-only simple cubic antiferromagnet.) In light of these decouplings, we cannot call this state a (1/2, 1/2, 0) cuboctahedral; it is merely a particular configuration out of a degenerate family that also includes collinear states.

V. CONIC SPIRAL STATES

The conic spiral states are generically incommensurate and constitute the most common class of non-coplanar state that we found. They are layered states, where the spins are all parallel in a given layer. That is, the lattice breaks up into layers, normal to some stacking direction $\hat{\mathbf{Q}}_{stack}$ in real space. We encountered only $\hat{\mathbf{Q}}_{stack} = \{Q00\}$ stacked conic spirals, so we concentrate on that case, but stacking directions other than $\{100\}$ should be feasible in principle. Within each layer, all the spin directions are the same; as you look in each successive layer, the spin directions rotate around an axis $\hat{\mathbf{c}}$ in spin space. Due to this layering, it is possible to map a conic state to a one-dimensional "chain lattice" (as introduced in Sec. V B), which is a significant simplfication in the analysis.

Considered from the LT viewpoint, a conic spiral is a mix of two different modes: two spin components follow an incommensurate wavevector $\mathbf{Q}$, spiraling as in a helimagnet, and the third component follows a commensurate wavevector $\mathbf{Q}'$ ($\mathbf{Q}' \cong 0[AF]$ in the asymmetric-conic case). In both $\mathbf{Q}$ and $\mathbf{Q}'$, all components transverse to the stacking direction must be zero.

A. Categories of conic spiral states

The conic spirals divide into subclasses, the alternating and asymmetric conic spirals, according to whether they are symmetric under the (spin space) symmetry of reflecting in the plane normal to $\hat{\mathbf{c}}$. In the octahedral lattice, the only type of conic spiral we observed was the asymmetric conic. However, in the chain lattice we find that two distinct classes of conic spiral are possible: the asymmetric conic and the alternating conic. In principle, both states should be possible in the octahedral lattice, but an analysis in terms of stacking vectors (see Sec. V B) reveals that longer range couplings ($J_5, J_6, \ldots$) would be necessary to stabilize the conics.

1. Asymmetric conic spiral

In the asymmetric conic, the ground states are linear combinations of helimagnetic and ferromagnetic modes. Let the stacking direction be along the z axis, so all spins are only functions of z. (Alternatively, we could interpret z as the position in the one-dimensional chain lattice of Sec. V B, below.) The helimagnetic part is parametrized with a rotating unit vector:

$$\hat{\mathbf{A}}(z) \equiv \cos(Qz)\hat{\mathbf{A}}_0 + \sin(Qz)\hat{\mathbf{B}}_0 \qquad (5.1)$$

where $(\hat{\mathbf{A}}_0, \hat{\mathbf{B}}_0, \hat{\mathbf{C}})$ form an orthonormal triad. Then

$$\mathbf{s}(z) = \cos(\alpha)\hat{\mathbf{A}}(z) + \sin(\alpha)\hat{\mathbf{C}}; \qquad (5.2a)$$

$$\mathbf{s}(z + \frac{1}{2}) = \cos\beta\hat{\mathbf{A}}(z + \frac{1}{2}) - \sin(\beta)\hat{\mathbf{C}}, \qquad (5.2b)$$

with $0 \leq \alpha, \beta \leq \pi/2$. The spins in each sublattice rotate about some common cone axis $\hat{\mathbf{C}}$ in spin space; spins of the same sublattice have the same component along the cone axis (giving net magnetic moments for both sublattices of $N * \mathbf{s}_{\parallel}^{(\alpha)}$, where $\mathbf{s}_{\parallel}^{(\alpha)}$ is the component of a spin of sublattice α along the common axis). The different sublattices are antiferromagnetically coupled, so these net moments have different signs. And because the couplings within the sublattices are not equal to those of the other sublattice, the magnitude of the net moments are not equal. This can be easier to understand if we think in terms of common-origin plots (see Figure 1), since then the spins all lie upon the surface of a sphere. In the common origin plot, each sublattice forms a cone. These cones are along the same axis, but oppositely oriented and their azimuthal (conic) angles are not equal.

2. Alternating conic spiral

In the alternating conic, one sublattice is a *planar* spiral, while the other is always a combination of the same helimagnetic mode and an antiferromagnetic mode. This state is thus represented, again using (5.1):

$$\mathbf{s}(z) = \cos(\alpha)\hat{\mathbf{A}}(z) + (-1)^z \sin(\alpha)\hat{\mathbf{C}}; \quad (5.3a)$$

$$\mathbf{s}(z + \frac{1}{2}) = \hat{\mathbf{A}}(z + \frac{1}{2}); \qquad (5.3b)$$

where $0 \leq \alpha \leq \pi/2$ for the alternating conic. Returning again to our common-origin plot (see Figure 1), one sublattice forms a great circle along the equator of the sphere. The other sublattice now traces cones on each side of this equator (the common axis is the vector normal to the circle). The spins of the second sublattice alternate between the two sides of the equator, giving the antiferromagnetic component. Thus, the difference between sublattices is more fundamental in the case the alternating conics than in asymmetric conics.

3. Splayed States

There are two other states essentially related to these conic spirals, but are important enough to deserve their own names (this is much the same as ferromagnetism being a special case of helimagnetism). We term these states ferromagnetic and ferrimagnetic splayed states.

Consider the alternating conic in the limit of the polar angle going to 0 or 1/2. In both cases, the spins are confined to a plane, but they are emphatically not in a helimagnetic configuration. The sublattice that was helimagnetic is now ferromagnetic and the sublattice that was conic now merely alternates (that is, reflects about equatorial plane without rotation). If the polar angle is 0 (1/2), then the dot product of spins in different sublattice is positive (negative) and the state is a ferromagnetic (ferrimagnetic) splayed state.

While the difference between ferromagnetic and ferrimagnetic splayed state seems rather trivial here, it is more dramatic when we think of asymmetric conics. The ferrimagnetic splayed state is produced when one of the conic angles and the polar angle go to 1/2 while the other conic angle remains arbitrary. But because the coupling between sublattices is antiferromagnetic for the asymmetric conic, the conic angles of the sublattices will always confine spins to opposite sides of the "equator." This means that the asymmetric conic will never continuously transform into a ferromagnetic splayed state, and so such a transition would necessarily be first order.

B. Stackings and chain mapping

For the cases of incommensurate conic spirals, our main analytic method is variational: we assume a functional form for the spin configuration (based on interative minimization results) depending on several parameters, and optimize exactly with respect to them. Say we know that the correct ground state is stacked a stack of planes with identical spins $--$ in practice this is determined empirically from the outcome of iterative minimization (Sec. II B) – then the variational problem is equivalent to a one-dimensional (and hence simpler) one: layers of the 3D lattice may be mapped into a chain containing inequivalent sublattices.

This mapping is fruitful in two or three ways. First, we could (and did) explore the chain lattice ground states using interative minimization, in much longer system lengths than would be practical in an $L \times L \times L$ system. Second, it is unifying, in that various stackings of various three-dimensional lattices map to the same chain lattice. Finally, it illuminates what conditions are necessary in order to obtain non-coplanar states.

Notice that if a stacked state is the true ground state of the three-dimensional lattice, its projection must be the true ground state of the chain projection (since the chain lattice states correspond exactly to a subset of three-dimensional states); but of course the converse is false: the proven optimal state of the chain lattice might be irrelevant to the three-dimensional lattice, when a different (e.g. unstacked) kind of ground state develops a lower energy. As coupling parameters are varied, that different state might become stable in a first-order transition; our only systematic ways to address that possibility are (i) iterative minimization (ii) watching for an exchange of stability between two LT eigenmodes at different wavevectors. And even with this method, we had to rely primarily upon iterative minimization for reliable results, as LT analysis is insufficient to determine the ground state, particularly in cases where a ground state cannot be constructed from the optimal LT modes.

For the cases that concern us here, the chain lattice has a basis of two sites per cell, with inversion symmetry at each site; we take the lattice constant to be unity. The mappings to

chain sites z is given by

$$z = \hat{\mathbf{Q}}_{\text{stack}} \cdot \mathbf{r} \qquad (5.4)$$

where $\hat{\mathbf{Q}}_{\text{stack}}$ is a vector of integers, having no common factor. We let "even" sites be those with z integer and "odd" sites be those with $z = \text{integer}+1/2$. As in three dimensions, we consider inter-sublattice couplings j_1 and j_3, as well as intra-sublattice couplings out to distances 1 and 2, namely j_2 and j_4 (between even spins) or j_2' and j_4' (between odd spins). Notice that, if $j_2 = j_2'$ and $j_4 = j_4'$, the chain system reduces to a Bravais lattice (with lattice constant 1/2) and its ground states are (at most) coplanar spirals, as explained in Sec. II A; that rules out $\hat{\mathbf{Q}}_{\text{stack}} = (1,1,1)$. Notice that for stackings in low symmetry directions (and thus requiring larger coefficients in the $\hat{\mathbf{Q}}_{\text{stack}}$ vector), short range J_{ij} couplings in the octahedral lattice map to long range j_{ij} couplings in the chain lattice, e.g. $\hat{\mathbf{Q}}_{\text{stack}} = (211)$ maps J_1 through J_4 to j_1 through j_6. Because longer range couplings quickly appear, it is reasonable to explore them in the chain lattice. In order to organize our exploration of parameter space, we shall call j_1, j_2, and j_2 "primary" couplings; j_3, j_4, and j_4' are "secondary" couplings, and if necessary are assumed small compared to the primary couplings.

We encountered $\hat{\mathbf{Q}}_{\text{stack}} = (1,0,0)$ stackings often enough in the iterative minimization, and we searched for $\hat{\mathbf{Q}}_{\text{stack}} = (1,1,0)$ type stackings also (although this search was ultimately unsuccessful). The $\hat{\mathbf{Q}}_{\text{stack}} = (001)$ mapping is illustrated in real space in Fig. 2. The numerical values of the mapped couplings is given by a matrix multiplication:

$$\begin{pmatrix} j_0 \\ j_1 \\ j_2 \\ j_2' \\ j_3 \\ j_4 \\ j_4' \end{pmatrix} = \begin{pmatrix} 4 & 2 & 4 & 0 & 4 & 2 \\ 8 & 0 & 0 & 16 & 0 & 0 \\ 0 & 0 & 2 & 8 & 4 & 4 \\ 0 & 1 & 0 & 0 & 4 & 0 \\ 0 & 0 & 0 & 0 & 0 & 0 \\ 0 & 0 & 0 & 0 & 0 & 0 \\ 0 & 0 & 0 & 0 & 0 & 0 \end{pmatrix} \begin{pmatrix} J_1 \\ J_2 \\ J_2' \\ J_3 \\ J_4 \\ J_4' \end{pmatrix} \qquad (5.5)$$

where j_0 is the energy within a plane of constant z in the octahedral lattice. Notice that, for this stacking vector, couplings J_1 through J_4 are projected down to j_0 through j_2. This helps explain the absence of stable conics in the octahedral lattice. We only find conics in the chain lattice for j_3 or longer-range couplings. But for this stacking $\hat{\mathbf{Q}}_{\text{stack}} = (001)$, require at least a J_5 coupling to generate an analogous coupling (for the alternating conic, J_6 is more likely, given the asymmetry between the sublattices).

C. Transversely modulated spirals

This is a hypothetical (but likely) class of states. Here "transversely modulated" means that when we decompose the lattice as a stacking of layers, a single layer does not have a single spin direction, but instead a pattern of spin directions. Whereas the asymmetric conic spiral used ordering wavevectors (say) $(Q,0,0)$ and $(0,0,0)$, and the alternating conic spi-
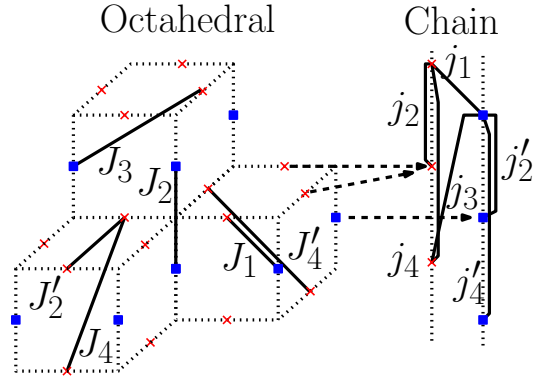

FIG. 2: (COLOR ONLINE) The mapping between the octahedral and chain lattices for a (001) stacking direction. All sites with the same value of z on the x and y sublattices (red x's) are projected onto the same point, while those in the z sublattice (blue squares) are mapped onto a different point (again a function z). As such, there are twice as sites mapped onto any x as there are mapped onto a square. The spatial structure is shown in dotted lines, while couplings are shown in solid lines.

ral used $(Q,0,0)$ and $(1/2,0,0)$, a transversely modulated spiral might replace the first wavevector by e.g. $(Q, 1/2, 1/2)$.

Equivalently, if we look at a column of successive cells along the stacking direction, in a plain conic spiral (whether alternating or asymmetric), adjacent columns are in phase, but in the transversely modulated conic spirals, different columns are offset in phase according to a regular pattern. It should be possible to generalize the chain mapping to such cases, but we have not tried it.

VI. DOUBLE-TWIST STATE

Here we describe the incompletely understood "double-twist" state, which has attributes in common with both cuboctahedral and conic states, and was observed only for a small set of couplings ($J_1 = -2$, $J_2 < 0$, $J_3=1$, all others zero). These couplings were selected to give $\mathbf{Q}_{\text{LT}} = (Q,Q,0)$, as the ground states previously encountered had a $\mathbf{Q}_{\text{LT}}$ either along the (111) direction or on the edges of the Brillouin zone. For a given Q, the value of J_2 is determined by:

$$J_2 = 4\sqrt{2} \cdot (3\cos^2(Q/2) - 1)/\sqrt{1 - 2\cos^2(Q/2)}. \quad (6.1)$$

We particularly studied the $Q = 3/8$ case. (Note that iterative minimization necessarily probes commensurate states, due to our boundary conditions.) This corresponds to $J_2/J_3 = -3.7717$, according to Eq. (6.1).

The double twist state is, to good approximation, composed solely of $(Q,Q,0)$ modes (for normalization, there will necessarily be other wave-vectors, but these have relatively small amplitudes). Unlike previous states, each sublattice has nonzero contributions from all $(Q,Q,0)$ wavevectors, rather than a subset. The weight of each sublattice in a given $(Q,Q,0)$ mode differs between sublattices, approximately in proportion to relative weight in the LT optimal mode with a similar $\mathbf{Q}_{\text{LT}}$.

The spatial variation produced by this combination of modes is complicated. There is a stacking axis in real space, which we take to be $\hat{z}$ without loss of generality. Spin space is characterized by three orthonormal basis vectors: $\hat{\mathbf{C}}$ defines a conic axis, around which the other two basis vectors $\hat{\mathbf{A}}$ and $\hat{\mathbf{B}}$ rotate as a function of z:

$$\hat{\mathbf{A}}(z) = \cos(Qz)\hat{\mathbf{A}}_0 - \sin(Qz)\hat{\mathbf{B}}_0; \quad (6.2a)$$

$$\hat{\mathbf{B}}(z) = \sin(Qz)\hat{\mathbf{A}}_0 + \cos(Qz)\hat{\mathbf{B}}_0; \quad (6.2b)$$

$$\hat{\mathbf{C}} = \hat{\mathbf{A}}(z) \times \hat{\mathbf{B}}(z) = \hat{\mathbf{A}}_0 \times \hat{\mathbf{B}}_0. \quad (6.2c)$$

We can parameterize this cartoon of the double twist state as

$$\begin{pmatrix} S_1(\mathbf{r}) \\ S_2(\mathbf{r}) \\ S_3(\mathbf{r}) \end{pmatrix} = \Gamma_0 \begin{pmatrix} -a & b & b \\ b & -a & b \\ b & b & -a \end{pmatrix} \begin{pmatrix} \sin(\Phi_y)\hat{\mathbf{A}}(z) \\ \sin(\Phi_x)\hat{\mathbf{B}}(z) \\ \Gamma\cos(\Phi_x)\cos(\Phi_y)\hat{\mathbf{C}} \end{pmatrix}$$
$$(6.3)$$

with $\Phi_x(c) \equiv Qx - \phi_x$, where ϕ_x is an arbitrary phase, similarly $\Phi_y(y) \equiv Qy - \phi_y$. Note the coordinates $\mathbf{r}$ in $\mathbf{S}_i(\mathbf{r})$ are the actual sites for sublattice i, which are half-odd-integers in the i component. Thus, addition to the twisting of the basis vectors along the stacking direction, in (6.2), there are spatial modulations transverse to the stacking direction that appear in the coefficients of $\hat{\mathbf{A}}, \hat{\mathbf{B}}$ and $\hat{\mathbf{C}}$ in (6.3)

While the form described by (6.3) is close to what we observe with iterative minimization, it unfortunately does not satisfy normalization: the ground state necessarily contains admixtures of non-optimal modes. (To satisfy normalization using only the $(Q, Q, 0)$ modes would require four-component spins.) In Eq. (6.3), $(-a, b, b)$ should ideally be the amplitudes (on the three respective sublattices) of the LT eigenvector at $(0, Q, Q)$, while Γ is a weighting factor that reduces the deviations of the spins in (6.3) from uniform normalization.

What if we demanded, not normalization of all spins, but only that the mean-squared value of $|\mathbf{S}_i(\mathbf{r})|^2$ be one in each sublattice? Since each cosine or sine factor has mean square of 1/2, and since $a^2 + 2b^2 = 1$, we ought then to have $\Gamma_0 = \Gamma = \sqrt{2}$. Projecting the actual result of iterative minimization onto such modes gave $\Gamma \approx 1.36$. Also, whereas $b/a = 1.64$ in the actual LT eigenvectors, we found $b/a \approx 1.5$ in the results of iterative minimization.

The double twist state can be viewed as related to the hypothesized transversely-modulated conics or to the cuboctahedral states. In particular, the composition of this state in terms of LT modes is more similar to the cuboctahedral states than to any other configuration.

The LT mode underlying this state, according to (6.1), has a continuously variable wavevector as J_2 is varied. Due to the limitations of iterative minimization with periodic boundary conditions, we have not followed the evolution of the double-twist state; in particular, we do not know if it becomes incommensurate in both the stacking (z) direction and the transverse directions.

VII. PHASE DIAGRAMS

To understand how the ground states outlined in Sec. III,IV, V, and VI fit together, it is necessary to examine the phase diagrams of the octahedral and chain lattices. A series of representative cuts through the phase diagrams for both lattices gives us a general sense of their topology, and specifically in what regions non-coplanar states are stabilized.

Of course, rescaling the couplings by any positive factor gives an identical ground state (with energy rescaled by the same factor). Therefore we present the phase diagrams in rescaled coordinates, normally $J_i \to J_i/|J_1|$ (except when $J_1 = 0$).

An important aspect of all the phase diagrams is the classification of the transitions into first-order (discontinuous), encompassed (continuous), or degenerate: the distinction between the last two kinds was explained in Sec. II D. Whenever a continuous manifold of degenerate states is found (always on a phase boundary), it is labeled in the diagrams by "$O(L^d)$" representing how the number of parameters (needed to label the states) scales with system size.

A. Octahedral Lattice

In the octahedral lattice we are fortunate in that most kinds of states have energies that can be written exactly as a linear combination of couplings (given in Table I [49]); the phase boundaries between such phases are simply the lines (more exactly hyperplanes) where the two energy functions are equal. Most other phase boundaries are handled analytically, e.g. the helimagnetic state and its "encompassed" ferromagnetic and antiferromagnetic states. The only phase boundary *not* determined analytically from a variational form was the double-twist state, for which we do not have an exact variational form; in this case the boundary was approximation by the LT phase boundary. We would expect that approximation to be accurate for any such complex phase that is built entirely from a star of symmetry-equivalent modes, provided the neighboring phase is built from other modes.

Using this information, we can easily find the phase boundaries of various states. To aid in graphical display, we will normalize all couplings by $|J_1|$ and restrict attention to $|J_3|/|J_1| < 1$. Phase diagrams will be plotted in the variables (J_2, J_2') representing a slice with (J_1, J_3) fixed. In all such slices, the second, third, and fourth quadrants of the phase diagram are dominated by antiferromagnetic phases of ordering vector $(1/2, 1/2, 0)$, $(1/2, 1/2, 1/2)$, and $(1/2, 0, 0)$ respectively. Recall that all of these are *nontrivially decoupled* states, in which distinct sublattices can be independently rotated due to cancellations of the inter-sublattice interactions. When thermal or quantum fluctuations are added to the description, "order-by-disorder effects" [3, 4] typically select specific states from these manifolds that are *collinear*. The first quadrant is dominated either by the ferromagnetic phase, or (if $J_1 < 0$) by the 120° 3 sublattice phase. Cuboctahedral phases may be found near the $J_2' = 0$ axis when $J_2 > 0$.

The phase transitions are always first order in the octahedral

State	$\mathbf{Q}$	Energy/spin
— Ferromagnetic	(000)	$-4J_X - J_2 - 2J_2' - 4J_4 - 2J_4',$ $J_X \equiv J_1 + 2J_3$
3 sublattice - 120°	(000)	$2J_X - J_2 - 2J_2' - 4J_4 - 2J_4'$
(1/2,1/2,0)-AFM	$(\frac{1}{2}, \frac{1}{2}, 0)$	$-J_2 + 2J_2' - 4J_4 - 2J_4'$
(1/2,1/2,1/2)-AFM	$(\frac{1}{2}, \frac{1}{2}, \frac{1}{2})$	$J_2 + 2J_2' - 4J_4 - 2J_4'$
(1/2,0,0)-AFM	$(\frac{1}{2}, 0, 0)$	$J_2 - 2J_2' - 4J_4 - 2J_4'$
$\pi/3$-Cuboctahedral	$(\frac{1}{2}, 0, 0)$	$-2J_1 - J_2 + 4J_3 + 4J_4$
$2\pi/3$-Cuboctahedral	$(\frac{1}{2}, 0, 0)$	$2J_1 - J_2 - 4J_3 + 4J_4$
Helimagnet	(qqq)	$-2J_1 - 2J_4 - J_4' - J_S^2/(8J_L),$ $J_S \equiv 2J_1 + J_2 + 2J_2' + 4J_3$ and $J_L \equiv 2J_3 + 2J_4 + J_4'$

TABLE I: Ground States of the Octahedral Lattice, with ordering wavevector $\mathbf{Q}$.

lattice, with the following exceptions, which can be classified according to the three scenarios for bridging states outlined in Sec. II D (encompassing and degenerate).

(1) The transition from the helimagnet to either the (1/2,1/2,1/2) antiferromagnet or to the ferromagnet is continuous, since the optimal wavevector varies continuously along (q, q, q) until it hits the commensurate value ((1/2,1/2,1/2) or (0,0,0)), then stops; this is an example of an encompassing state.

(2) Transitions between two antiferromagnet phases are always degenerate, since the phase boundaries in parameter space are given by $J_2=0$ or $J_2'=0$, which (trivially) decouple sublattices (implying a degenerate family of states). In the Brillouin zone, the wavevector can evolve continuously along (1/2,q,k) and (1/2,1/2,q) (for the (1/2,0,0) and (1/2,1/2,0) antiferromagnets, respectively).

(3) Lastly, transitions between states of the same $\mathbf{Q}_{LT}$ are degenerate, occurring where two eigenvalues of the LT matrix for $\mathbf{Q}_{LT}$ cross, as a function of changing parameters. This is found for the (0,0,0) modes (ferromagnetism and the 120° state) and the (1/2,0,0) modes (both types of cuboctahedral states with each other and with the $\mathbf{Q}_{LT} = (1/2, 0, 0)$ antiferromagnetic state). Because the degeneracy is limited to different eigenmodes of the same wavevector, these are $O(L^0)$ degenerate transitions.

Consider first the phase diagram produced with ferromagnetic J_1 and no couplings beyond J_2, J_2' (Figure 3). In this case, we find only four states, all of them coplanar (these are outlined in III). What's particularly important here, though, is the way that the phase diagram divides up into four quadrants. This is a fairly generic feature that we will see in other phase diagrams. Along the $J_2' = 0$ line between the (1/2,1/2,1/2) AFM and the (1/2,0,0) AFM, in all the phase diagrams, we get a degenerate ($O(L^2)$) decoupled state, in which each J_2'-coupled line has an independent staggered spin direction.
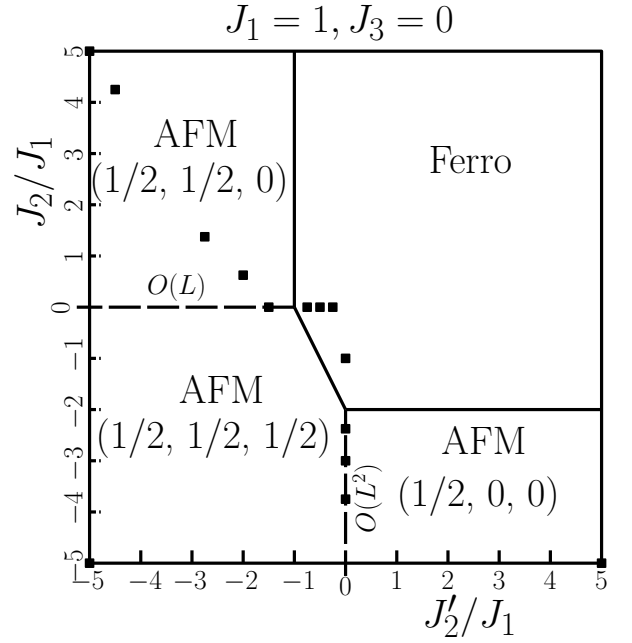

FIG. 3: Octahedral Phase Diagram for $J_1 = 1$, $J_3 = 0$. Squares indicate couplings tested with iterative minimization. Solid lines denote first order transitions, dashed lines denote degenerate transitions (Sec. II D), where the scaling of degrees of freedom is labeled. Dotted lines indicate a second order transition from encompassing states. Regions shaded gray indicate a non-coplanar phase.
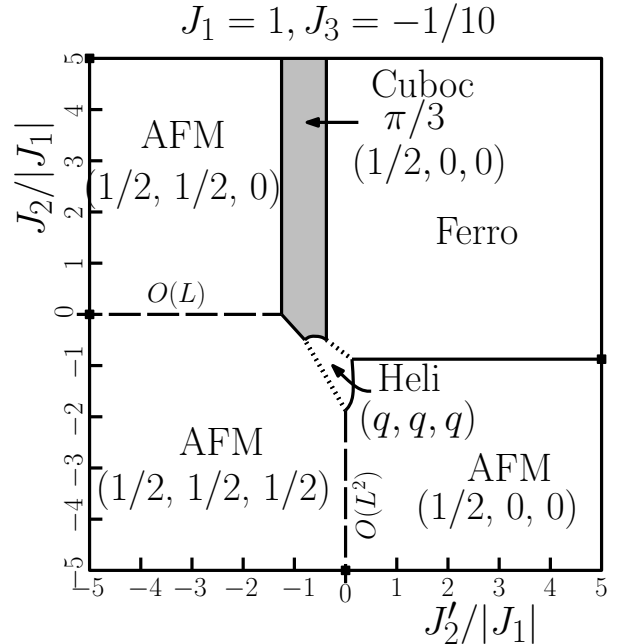

FIG. 4: Octahedral Phase Diagram for $J_1=1$, $J_3 = -1/10$. First instance of a non-coplanar state (the $\pi/3$ cuboctahedral state, in the shaded region) and of helimagnetism.
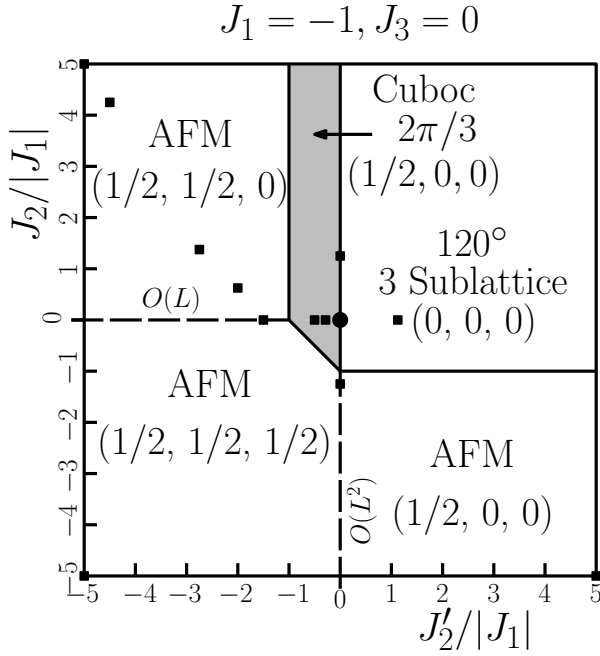
FIG. 5: Octahedral Phase Diagram for $J_1 = -1$, $J_3=0$. First instance of the $2\pi/3$ cuboctahedral state. The large circle point is the case of only J_1 couplings, corresponding to the (highly degenerate) $120°$ state.
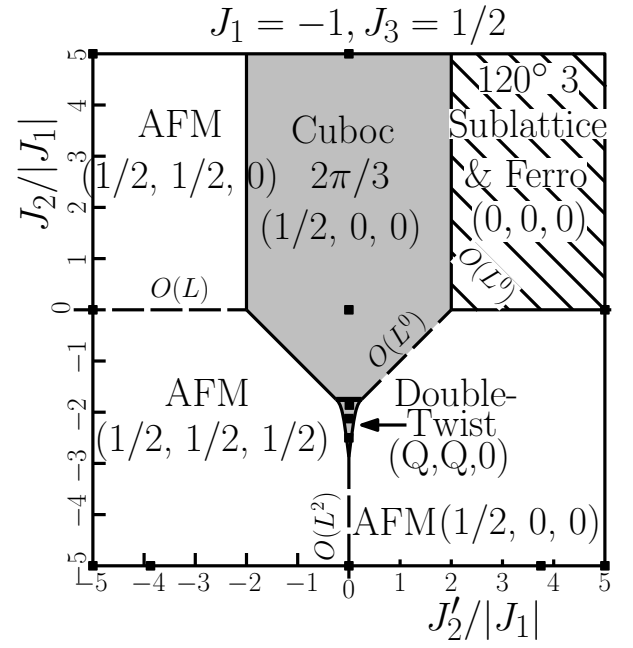

FIG. 6: Octahedral Phase Diagram for $J_1 = -1$, $J_3=1/2$. The double-twist state is found in the small region near the origin. The striped region indicates this slice ($J_3 = 1/2$) contains a phase boundary between the $120°$ 3-sublattice and ferromagnetic states; for the parameter set plotted, that region has states of the degenerate (marked "$O(L^0)$") parameters) and nontrivially decoupled kind. If we varied J_3 to pass through that region of parameter space, we would cross a degenerate phase transition.

Let's now examine how the ferromagnetic J_1 phase diagram is modified by an antiferromagnetic J_3 (Figure 4). First of all, it stabilizes the $\pi/3$ cuboctahedral state, our first example of a non-coplanar phase. J_3 also stabilizes a (q, q, q) helimagnet at the center of the phase diagram. The boundaries of this phase are quite sensitive to J_3: as J_3 becomes more antiferromagnetic, the helimagnet's phase boundaries with ferromagnetism and $(1/2,1/2,1/2)$ antiferromagnetism move outward in opposite directions, so as to increase the region of parameter space that is helimagnetic. Meanwhile, the phase boundaries of helimagnetism with the $(1/2,0,0)$ antiferromagnet and $\pi/3$ cuboctahedral state move *inwards* in opposite directions, so as to decrease the region of parameter space that is helimagnetic. The result is that, as J_3 becomes more antiferromagnetic, the helimagnetic region of parameter space first grows and later shrinks until $J_3=-J_1/2 < 0$, where it disappears entirely.

Now we turn to the phase diagrams with antiferromagnetic J_1, first considering arbitrary J_2, J_2' with $J_3 = 0$ (Figure 5). In this case, we still see the quadrant structure, at least qualitatively; the upper right quadrant now represents the (ordered) three-sublattice $120°$ state. However, a strip between the upper quadrants is occupied by the $2\pi/3$ cuboctahedral state, a non-coplanar state which only requires two non-zero couplings. Furthermore, we find the (highly degenerate) "J_1-only" state along the boundary between the $2\pi/3$ cuboctahedral state and the three-sublattice $120°$ state. It is interesting to note that at this point in parameter space, the type of transition changes. Because of the vanishing of the couplings, the minimum eigenvalue is a constant along (q,0,0). This makes the phase transition at this point a degenerate ($O(L^1)$), con-

tinuous transition, even though it is elsewhere first order.

For antiferromagnetic J_1 adding ferromagnetic J_3 (Figure 6), we see the $2\pi/3$ cuboctahedral state expand, changing the topology of the phase diagram (it now shares a boundary with the $(1/2, 0, 0)$ antiferromagnet). In addition, near the triple point of the $(1/2, 1/2, 1/2)$ antiferromagnet, $(1/2, 0, 0)$ antiferromagnet and $2\pi/3$ cuboctahedral state, we find the double twist state [50]. Note that the slice of parameter space shown here, $J_1 = -2J_3$, includes the phase boundary between the three-sublattice $120°$ state and the ferromagnetic state, and on the boundary has an extra degeneracy of the kind described in Sec. II D.

The double-twist can be understood as a selection from the family of degenerate states. Along the $J_2' = 0$ line (boundary), we have a degenerate form of decoupled state: sublattices decouple by row, giving a large degeneracy of ground states. However, this decoupling depended upon the alternating order within each sublattice which led to cancellations. A spiral distortion (selected by adding J_1, J_3 to J_2 only state, with J_2 sufficiently small) within a sublattice allows a non-cancelling interaction between it and another sublattice, which lowers the energy.

The $J_1 < 0$ phase diagrams superficially resemble the the $J_1 > 0$ phase diagrams, with two different cuboctahedral states appearing around the $J_2 > 0$ axis, and a helimagnet or double-twist state (respectively) appearing in a small edge below the phase diagram's center.

We have also considered the case of $J_1 = 0$ with an antiferromagnetic J_3 (phase diagram not shown). This phase diagram, apart from the trivial change of normalizing the couplings by $|J_3|$ instead of $|J_1|$, strongly resembles the case of antiferromagnetic J_1 and $J_3 = 0$ shown in Figure 5); the sole difference is that we now find the $\pi/3$ cuboctahedral state in place of the $2\pi/3$ cuboctahedral.

Iterative minimization found asymmetric conic states along the phase boundary between the (1/2,1/2,1/2) antiferromagnet and the (1/2,0,0) antiferromagnet, but we believe these are artifacts, in the sense we will describe. This boundary corresponds to LT modes degenerate over a plane of wavevectors, leading to a degenerate family of spin ground states with an arbitary wavevector. These are generically non-coplanar spirals, except the limiting states of this family are collinear "encompassed states" (in the nomenclature from Sec. II D). Thus, although these conic spirals are valid ground states, we do not count them as non-coplanar, since that is not *forced* by the couplings. This is an instance where the overlap between "encompassing" and "degenerate" states is especially stark, as the family of degenerate states coincides with the class of encompassing states.

The impossibility of forcing *any* conic spiral in the octahedral lattice is understood by using the mapping (5.5) of couplings from the octahedral lattice to the chain lattice (see Sec. V B). We will see shortly (Sec. VII B) that stabilizing either kind of conic requires a coupling j_3 or j_4 in the chain lattice; for a (100) stacking vector, Eq. (5.5) takes octahedral couplings J_1 through J_4 to chain-lattice couplings j_0 through j_2, so clearly couplings J_5, J_6 or longer are required (and sufficient) to truly stabilize conic spirals in the octahedral lattice.

B. Chain Lattice

The chain lattice ground states are significantly more complicated than those of the octahedral lattice. Analytically determining the optimal energy of even the helimagnet becomes difficult when couplings beyond j_3 are included. Therefore, while we can easily determine a variational form for the energies, we cannot analytically determine the ground state when couplings j_3 or higher are introduced. Energies are given in table II, which are then numerically optimized to give the subsequent phase diagrams. We once again normalize by $|j_1|$, but we now plot $j_2'/|j_1| \times j_2/|j_1|$, rather than $J_2/|J_1| \times J_2'/|J_1|$. This change of convention does not have great physical implication, as the difference between J_2 and J_2' in the octahedral lattice is distinct from the difference between j_2 and j_2'. Lastly, by the definitions of the chain lattice, several properties of the phase diagram follow immediately. First, simultaneous exchange of j_2 with j_2' and j_4 with j_4' will merely change the labeling convention to distinguish the two sublattices. The ground state in the chain lattice must therefore be invariant under this operation. Furthermore, when $j_2 = j_2'$ and $j_4 = j_4'$, this exchange will not change anything. In this region of parameter space, there is no difference between the two sublattices and the chain lattice becomes a Bravais lattice with unit cell 1/2. From this fact and Sec. II A, it follows that

State	Q	Energy
Ferro	0	$-2j_1 - j_2 - j_2' - 2j_3 - j_4 - j_4'$
AFM	0	$2j_1 - j_2 - j_2' + 2j_3 - j_4 - j_4'$
Heli-magnet	2ψ	$-2j_1 \cos\psi - (j_2 + j_2') \cos 2\psi$ $-2j_3 \cos 3\psi - (j_4 + j_4') \cos 4\psi$
splayed ferro	0 and 1/2	$(j_1 + j_3)^2/2j_2 + j_2 - j_2' - j_4 - j_4'$
splayed ferri	0 and 1/2	$(j_1 + j_3)^2/2j_2 + j_2 - j_2' - j_4 - j_4'$
Alter-nating Conic	1/2 and 2ψ	$-2(j_1 \cos\psi + j_3 \cos 3\psi) \cos\alpha$ $+j_2 - j_4 - j_2' \cos 2\psi - j_4' \cos 4\psi$ $-(j_2[\cos 2\psi + 1] + j_4[\cos 4\psi - 1]) \cos^2\alpha$
Asym-metric conic	0 and 2ψ	$-2(j_1 \cos\psi + j_3 \cos 3\psi) \cos\alpha \cos\beta$ $+2(j_1 + j_3) \sin\alpha \sin\beta - j_2 - j_2' - j_4 - j_4'$ $-(j_2 \cos^2\alpha + j_2' \cos^2\beta)(\cos 2\psi - 1)$ $-(j_4 \cos^2\alpha + j_4' \cos^2\beta)(\cos 4\psi - 1)$

TABLE II: Parametrizations and Energies of the Chain Lattice. Q denotes the ordering wavevector(s), as a multiple of 2π. The energy per unit cell is given. The splaying angle is given by $\cos\alpha = -(j_1 + j_3)/2j_2$ for the splayed ferromagnet or $+(j_1 + j_3)/2j_2$ for the splayed ferrimagnet.

states in this region are necessarily coplanar.

To classify phase boundaries in the chain lattice, it is important to consider limiting cases (i.e. encompassed states in the nomenclature of Sec. II D). States with variational parameters (the helimagnetic wave-vector q, as well as the conic/splay angles) will undergo a second-order transition when their parameters reach a limiting value (0 or 1/2 for the helimagnet angle, 0 or 1/4 for conic angles). Thus there is a second-order transition between helimagnetism and either antiferromagnetism or ferromagnetism, as well as between alternating conics and every other state (except asymmetric conic). Asymmetric conics, on the other hand, have second-order transitions to ferromagnetism, antiferromagnetism, helimagnetism, or ferrimagnetic splayed states, but not to ferromagnetic splayed states or alternating conics. The splayed states, meanwhile, can only have second-order transitions to ferromagnetism or antiferromagnetism (depending upon which type of splayed state it is), to the other splayed state, or the appropriate conics. All other transitions are necessarily first-order.

Consider first the case of j_1 ferromagnetic with no couplings beyond j_2, j_2' (Figure 7). The phase diagram displays the same quadrant structure that we found in the octahedral lattice. However, the quadrant structure is not identical in the two lattices. First of all, the ground states are different in the chain lattice (helimagnetism and splayed states instead of various forms of antiferromagnetism). Secondly, the topology of the first and second order transitions are reversed for the two lattices. Both of these phenomena can be explained by appealing to the additional degrees of freedom in the octahedral lattice. Because the octahedral lattice has three spatial variables, it has ground states that cannot exist in the chain lattice. This includes families of degenerate states at the phase boundaries
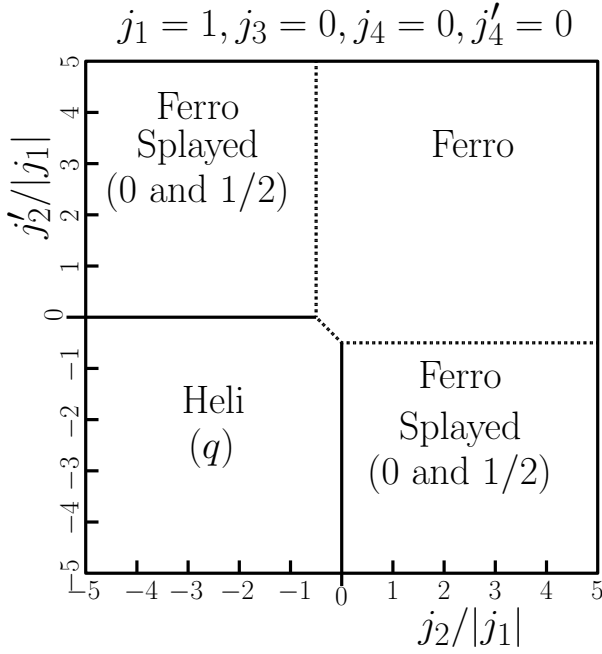
FIG. 7: Chain Lattice Phase Diagram for j_1=1, j_3=0, j_4=0, j_4'=0. Note similarity of phase boundaries to Figure 3, despite the lack of other similarity.

of the octahedral lattice, producing second order transitions (when there are second order transitions in the chain lattice, they are principally due to encompassing states).

Next, we examine the case j_1 antiferromagnetic and j_3 ferromagnetic (Figure 8). Several states in the quandrant structure are different from the ferromagnetic j_1 case (i.e. ferrimagnetic vs ferromagnetic splayed), but more interesting is the presence of the asymmetric conic - the first instance of a nonplanar state in the chain lattice. In much the same way that tuning j_3 in the octahedral lattice produced helimagnetic states around the phase boundaries of the more common states, so in the chain lattice do we find that the asymmetric conic state becomes stabilized around what would be the antiferromagnetic, ferrimagnetic splayed, helimagnetic triple point. And unlike the helimagnetic state in the octahedral lattice, which had both first order and second order transitions, the asymmetric conic has only second order transitions (this is because it is an encompassing parametrization of every other state in this slice of the phase diagram).

If we switch the sign of j_3 so that we have both $j_1 = -1$ and $j_3 = -0.28$ antiferromagnetic, the topology of the phase diagram (not shown) is much the same as Figure 8. The AFM/Heli boundary gets shorter and moves towards the lower left, so that the four domains almost meet at a point. More significantly, the asymmetric conic does not appear along the phase boundaries. Instead, all transitions are continuous, except that along both parts of FerriSplayed/Heli boundary, the portion closest to the center is first-order. [51] (The point where the nature of the transition switches from first-order to continuous is thus of tricritical type.)

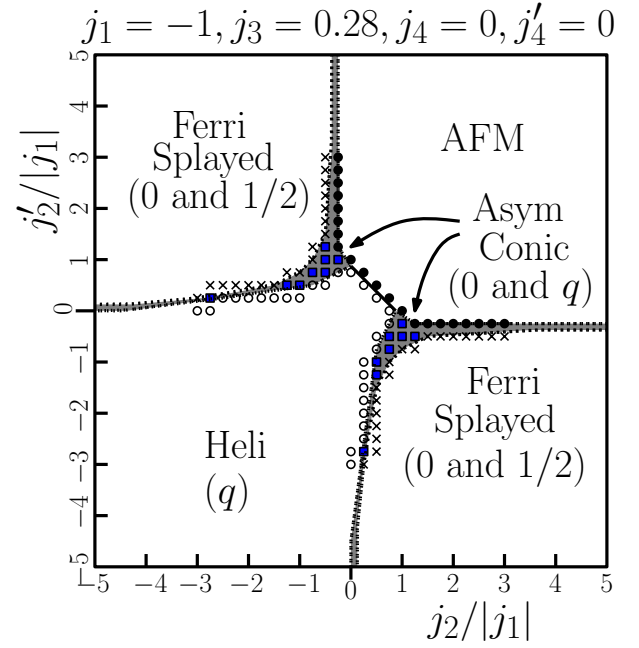Finally, we consider the case of j_1 ferromagnetic and j_4

FIG. 8: (COLOR ONLINE) Chain Lattice Phase Diagram for $j_1 = -1$, j_3=0.28, j_4=0, j_4'=0. First state with asymmetric conic, and therefore first instance of non-coplanar ground states in the chain lattice. White circles denote helimagnetic phase, black circles anti-ferromagnetic, crosses splayed ferrimagnetic, and filled squares (blue online) asymmetric conic, the phases determined by numerically optimizing the variational form of the energy for these couplings.
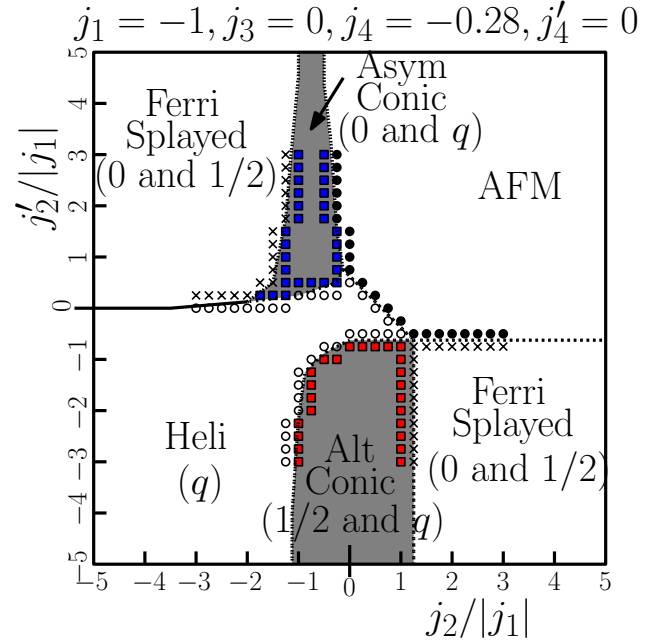

FIG. 9: (COLOR ONLINE) Chain Lattice Phase Diagram for $j_1 = -1$, j_3=0, $j_4 = -0.28$, j_4'=0. Filled squares denote conic spiral phases, of which both kinds exist in this parameter slice: symmetric conic in the upper half (blue online) and asymmetric conic in the lower half (red online). This is our first instance of an alternating conic.

antiferromagnetic (Figure 9). This slice of parameter space is quite interesting as both types of conics are present. Furthermore, the alternating conic now fills a relatively large region of parameter space. This is likely due to its highly non-linear dependence on j_4 (as a function of its variational parameters).

VIII.   CONCLUSION AND DISCUSSION

To conclude the paper, we first review our principal results, and then assess how much of what we learned is transferable to other lattices.

A.   Summary

The highlights of this paper include both concepts and methods, as well as results specific to the octahedral lattice, which seems relatively amenable to non-coplanar states. We pay special attention (Sec. VIII A 3) to commonalities in the positioning of non-coplanar states in the phase diagram vis-à-vis neighboring phases.

Our overall focus had a flavor of reverse engineering, in that we try to ask which couplings gave a certain phase (or which gave any non-coplanar phase) – of course in order to do that, one must also understand the forwards question (given the couplings, what is the phase). In that sense, our work is an example of a "materials by design" philosophy, whereby materials are tailored – e.g. by adjusting their chemical content – to have a combination of interactions leading to a desired state.

1.   Methods

Our basic recipe to determine the ground state of a non-Bravais lattice was a two-step process (Sec. II). First, an approximate ground state configuration is generated through iterative optimization (Sec. II B) of a lattice, starting from a random initial spin configuration. From this result, an idealized spin configuration is created. The idealized formulation, if it has parameters undetermined by symmetry, is then used variationally optimize the Heisenberg Hamiltonian (Sec. II C), yielding also the energy per site as a function of parameters. When this has been carried out for each candidate phase, a phase diagram (Sec. VII) can be generated.

We refined the basic recipe further using three additional concepts or tricks. First, although the eigenmodes of the coupling matrix do not (in the non-Bravais case) automatically lead us to the ground state, they sometimes do work and are always a useful guide. Second, if the magnetic structure is layered, the three-dimensional octahedral lattice can be mapped to various (non Bravais) one-dimensional lattices; such "chain" lattices are much more tractable than the cuboctahedral one, but they still support non-coplanar states. Third, we applied perturbation analysis to find second-order phase boundaries (especially in combination with variational optimization, but also in the Luttinger-Tisza Fourier analysis).

Namely, when a ground state could not be written exactly, but emerges as an instability of a closely related state – e.g. a helimagnetic phase out of the ferromagnetic one – we can expand around the latter state and solve for the couplings at which it goes unstable.

The insufficiency of finding regions with the correct $\mathbf{Q}_{\mathrm{LT}}$ for the purpose of stabilizing a targeted magnetic structures is an important caveat for the LT approach. There are some combinations of modes which *cannot* be stabilized by *any* set of pairwise interactions. That is, we can make them be optimal modes, but only if they are part of a degenerate family that includes other optimal LT modes that are unrelated by symmetry.

2.   Results

We identified two categories of non-coplanar arrangements (which could be defined for more general lattices than the octahedral one). First, there are the commensurate three-$\mathbf{Q}$ states, exemplified here by the highly symmetric "cuboctahedral" spin state (Sec. IV). A second general class includes several varieties of incommensurate "conic spiral" (Sec. V). The commensurate three-$\mathbf{Q}$ states were found for both short and long range couplings (i.e. J_i's limited to no more than second-nearest neighbors or extending beyond second-nearest neighbors), while incommensurate conic spirals were possible for our lattice only when there are some J_i's beyond the second neighbors.

The conic spirals came in "alternating" or "asymmetric" subclasses (stable in different parts of $\{J_i\}$ parameter space) according to whether the spin components along the rotation axis were the same in each layer or alternated. This suggested that an additional subclass should exist, the "transversely modulated conic spiral", which is non-uniform in each layer. In addition, we came across a "double-twist" ground state of high (but not cubic) symmetry, which has some commonalities with the cuboctahedral state but is probably best classified as a transverse-modulated conic spiral (Sec. VI).

The conic spiral states were found to be a function of one spatial coordinate, allowing the more involved octahedral lattice to be mapped to the 1D chain lattice while preserving the ground state (Sec. V B). While this mapping is not a generic property of ground states in the octahedral lattice, it dramatically simplifies the analysis. Moreover, the transformation provides a guide for the couplings required to stabilize the conic spiral states in the octahedral lattice.

Note that while the presence of inequivalent sublattices was necessary for the stabilization of non-coplanar states in the one-dimensional chain lattice, it is not so in higher dimensions. Our octahedral-lattice couplings explicitly treat all sites equivalently; non-coplanar states emerge either when it divides into unequal layers, that map to the chain lattice, or when it supports three-dimensional spin patterns not mappable to a chain lattice.

The most dramatic examples when the chain lattice fails to represent the ground state in the octahedral lattice are the cuboctahedral states, for which there is no distinguished di-

rection of variation (or stacking vector)

3. Why noncoplanar states are scarce

One might have expected noncoplanar ground states to be generic (in the non-Bravais case, when they are possible at all) but in fact they were seen in only a small portion of our parameter space (Sec. VII). In fact, non-coplanar phases typically appeared in the phase diagram as "bridges" intermediate between simpler phases; there are two scenarios of bridging, as formulated in Sec. II D.

First, typically along the phase boundary between two simple commensurate phases, one finds families of continuously degenerate states. Usually, this infinite family includes coplanar states but the generic member is non-coplanar; appropriate tuning of the couplings (e.g. including further neighbors) can select particular non-coplanar states in different ways. However, since the non-coplanar phase was limited (in the first-order description) to the (measure zero) boundaries between planar states, it naturally occupies only in a small region of the extended parameter space. Indeed, the non-coplanar states we found in the octahedral lattice either occurred in small wedges, e.g. the cuboctahedral or double-twist states or were only observed as accidental instances of the degenerate family in cases where the degeneracy cannot be broken (within the parameter space we took as the scope of this paper), e.g. the asymmetric conic states.

Second, there are the "encompassing states". Such states become qualitatively different as a free parameter reaches some limiting value (a canonical example is the collinear ferromagnet as a limiting case of planar spirals.) In the chain lattice, we often observed phase boundaries between two states that did not encompass each other; by tuning the couplings, it was sometimes possible to stabilize a third state which encompassed the original two, so the original first-order transition is converted to two successive second-order transitions with the encompassing state in the middle. This is the means by which conic spiral states are stabilized in the chain lattice.

Recently, a framework was proposed with a motivation similar to ours, the "regular states" [52] which have a magnetic symmetry such that all sites symmetry-equivalent. The cuboctahedral state is an example. However, this is neither necessary nor sufficient for our own problem, to find all kinds of non-coplanar states: most of those, e.g. the double-twist state, are not regular, and conversely certain non-coplanar regular states are not stabilized by bilinear exchange interactions alone.

B. Generalizations to other lattices?

Now we consider moving beyond the somewhat artificial octahedral lattice. We examine the necessary conditions for non-coplanar spin configurations analogous to the two main classes we discovered (cuboctahedral and conic spiral). Can our results be applied to other lattices, such as the pyrochlore lattice?

1. Generalizing the cuboctahedral state?

The cuboctahedral states seem highly specific to the octahedral lattice, since they possess the same symmetries as the lattice. On the other hand, the LT construction (each sublattice using different combinations of LT modes, the combinations being related by rotational symmetry of the different sublattices) seems fairly generic. A general name for states like the cuboctahedral state might be "commensurate triple-Q state", referring to its content of LT modes. Can such states be found in other lattices, or are there others in the octahedral lattice?

One answer requires that the hypothetical generalized state enjoys the full symmetry of the lattice, as the cuboctahedral state does. Then the number of site classes must be a multiple of the number of spin components, i.e. of three. That will not work for the pyrochlore lattice, in which there are *four* site classes associated with (111) directions. However, it might work in the half-garnet lattice, which has *six* site classes associated with (110) directions.

A second, more systematic way to answer question follows the LT approach of Sec. IV C. The state must be a linear combination of three modes – one for each component of spin. For the state to enjoy the full lattice symmetry, these must be the complete star of symmetry-related modes, thus it must have a threefold multiplicity. Furthermore, each mode must be real (otherwise one mode requires two spin components); that happens only if the wavevector is half a reciprocal lattice vector, i.e. is at the center of one of the Brillouin zone's faces.

However, Sec. IV C 1 gave a cautionary example: finding such modes is not *sufficient*, because it might give a state with decoupled sublattices, so that the cuboctahedral state would merely be one undistinguished configuration in a continuous manifold of degenerate states that even includes collinear states. We can, in fact, borrow a notion from Section V B to guess when this happens: mapping to a chain lattice, now applied to LT modes rather than to spin structures. The wavevector of one mode defines a set of planes, and thus a way of projecting both the sites and the mode onto a one-dimensional chain lattice. On the chain lattice, in order that the mode be real, the wavevector must be π. If all the site planes were equivalent, the chain lattice is a Bravais lattice and the mode must be a plane wave; with $Q = \pi$, it is easy to see we get a decoupled pattern, namely $(+1, 0, -1, 0, ...)$. In the octahedral lattice, the $\{1/2, 0, 0\}$ modes have a threefold degeneracy and also correspond to a non-equivalent set of stacked planes, giving a cuboctahedral state, whereas the threefold degenerate $\{1/2, 0, 0\}$ modes have equivalent stacked planes and give decoupled states. In the pyrochlore lattice, the $\{1, 0, 0\}$ modes have a threefold multiplicity but have equivalent stacked planes; on the other hand, the $\{1/2, 1/2, 1/2\}$ modes have inequivalent stacked planes but their multiplicity is fourfold. Thus, in the pyrochlore case this path does not lead us to a cuboctahedral state.

The third way to answer this question is via the cluster constuction of Sec. IV A, in which the lattice was decomposed into cuboctahedral cages. Indeed, some other lattices consist of a union of roughly spherical "cage" clusters: e.g., in the Cr_3Si-type or "A15" structure, the majority atoms form cages

in the form of distorted icosahedra. Furthermore, couplings can certainly be chosen such that the spin ground state of a cluster forms a the same polyhedron as the cluster itself.

However, our ground-state construction (Sec. IV A) demanded that the spin configurations in adjacent cages be related by a *reflection* in spin space. Thus the cages alternate between proper and improper rotations of a reference configuration. That is possible only if the cage centers form a *bipartite* lattice, which is not true for the A15 majority-atom cage centers. (They form a bcc lattice with first- and second-neighbor links.)

2. Generalizing the non-coplanar spirals?

Long ago, Kaplan and collaborators studied *doubly* magnetic spinels, and identified a (noncoplanar) "ferrimagnetic spiral" configuration arising from exchange interactions (a spiral of this sort is responsible for multiferroic properties of $CoCr_2O_4$ [18]. This is actually a kind of double spiral (each magnetic species accounting for one of the spirals). Notice that we could map that structure to a chain, too, and that chain would have two inequivalent sites, which we point out is a precondition for developing a noncoplanar state.

For a mapping to the 1D chain lattice to provide a non-coplanar state, the mapped sites must be inequivalent by translation; if not, the chain lattice is a Bravais lattice and must have (at most) a coplanar spiral state. This in turn depends on having *unequal* layers in the three-dimensional lattice, which is is impossible in the Bravais case, but inequivalent layers can emerge from a non-Bravais lattice with fully symmetric couplings. Thus, as we worked out in Sec. V B, a $\{100\}$ stacking in the octahedral lattice has twice as many sites on x and y bonds, constituting one kind of layer, as there are sites on z bonds, constituting the other kind.

The stacking direction is one in which the wavevector is incommensurate, and so we may seek out parameter sets for which $\mathbf{Q}_{LT}$ goes incommensurate in a desired direction. However, this is no guarantee that the actual ground state is stacked, since it might be better energetically to combine these modes (or ones nearby in $\mathbf{k}$-space) in a quite different way. Thus, although we found some optimal $\mathbf{Q}_{LT}$ wavevectors in directions other than $\{100\}$, they were never the basis of a stacked spiral.

C. On to pyrochlore lattice?

The pyrochlore lattice is undoubtedly the most prominent non-Bravais lattice that is likely to have non-coplanar states, and was a major motivation for the methods we developed in this paper for the more tractable octahedral lattice.

Relatively few works have tackled the isotropic spin problem on the pyrochlore lattice, beyond the (massively degenerate) case of only J_1 [analogous to the $J_1 = J_2$ case on the cuboctahedral lattice]. The J_1–J_2, or J_1–J_3 pyrochlore, with large antiferromagnetic J_1, has a noncoplanar and somewhat obscure state that is not fully understood at $T = 0$ [54–56].

In the spinel $GeNi_2O_4$, neutron diffraction found a $\{111\}$ ordering consisting of alternating kagomé and triangular lattice layers with different densities of spins, reminiscent analogous of the $\{100\}$ stackings we have explored in the octahedral lattice. Ref. 53 invoked interactions out to J_4 in order to rationalize this state, but did not verify it was the ground state for the suggested interactions. Finally, to address metallic pyrochlore compounds, a toy Hamiltonian was investigated on the pyrochlore lattice with exchange couplings having RKKY oscillations [57].

Very recently, a comprehensive study has been carried out for just the J_1–J_2 phase diagram of the pyrochlore lattice by applying the methods of the present paper, which were equally effective in that case [58]. About four complex states were identified, including that above mentioned state introduced by Kawamura and collaborators [54–56]; a state reminiscent of our double-twist state; a more complex generalization of a conic spiral; and a cuboctahedral spin state that has less than cubic lattice symmetry, thus evading the negative conclusions of Sec. VIII B 1 [58].

Appendix A: Perturbative Calculation of Phase Boundaries

To move from a collection of ground states discovered at discrete points in parameter space to draw a full phase diagram is non-trivial. To analyze the phase boundaries of the more complicated states (those with free parameters in their parametrization) we depend on either variational optimization (Sec. refsec:var), or some kind of perturbation theory. Perturbation theory can be applied in two places: either to the LT matrix, or to the Hamiltonian of a parametrized spin state. The former is more straightforward, but is limited since most of the non-coplanar ground states are not exactly built from optimal LT eigenmodes.

An obvious caveat for either of these applications of perturbation is that they detect continuous transitions, representing infinitesimal changes in the spins: it is a bifurcation of the local minima as points in the configuration space. But there the ground state might instead change due to a first order transition, when the energies of two separated configurations cross as parameters are varied. We do encounter the first-order case on occasion, though not nearly so often as the continuous one. To detect such discontinuous transitions, we must compare numerical calculations of the ground state energies.

Our original question was "given a certain set of parameters, what is the ground state", but in these calculations it

has been turned around to "given a particular ground state, for what parameter sets is it favored?"

1. LT Analysis (octahedral lattice example)

We give an example here of the use of perturbation theory to discover the incipient instabilities of LT modes. Such an approach may be especially useful to locate the phase boundaries for transitions from an LT exact ground state to more complicated, incommensurate states. If one is hunting for the parameter domain which would stabilize an particular mode with ordering wavevector $\mathbf{Q}$, a substitute problem is to find the parameter domain in which this mode (or one with $\mathbf{Q}_{\mathrm{LT}}$ similar to $\mathbf{Q}$) is the optimal LT mode. We reiterate the caveat from Sec. II A: such a discovery is a necessary but not sufficient criterion to guarantee the existence of any ground state based on the obtained $\mathbf{Q}_{\mathrm{LT}}$. (It is not sufficient because the actual ground state could feature additional modes or modes merely in the neighborhood of $\mathbf{Q}_{\mathrm{LT}}$.)

The LT matrix elements $J_{ij}(\mathbf{k})$ and eigenvalues $\tilde{J}(\mathbf{k}\nu)$ are functions of wavevector $\mathbf{k}$. Imagine that $\mathbf{Q}_0$ is a point of high symmetry in the zone so as to be a stationary point for $\tilde{J}(\mathbf{k}\nu)$. For some parameter sets, we know, it is a minimum and in fact optimal; whereas for some other parameter sets, we imagine, it is only a saddle point, and the minimum occurs at some nearby wavevector of lower symmetry.

One first writes a Taylor expansion of the LT matrix in powers of $\delta\mathbf{k} \equiv \mathbf{k} - \mathbf{Q}_0$. Using standard techniques (formally identical to those used for eigenfunctions of the Schrödinger

equation) it is straightforward to write a perturbation expansion for $\tilde{J}(\mathbf{k}\nu)$ in powers of $\delta\mathbf{k}$. Inspection then shows where this stops being positive definite. Since the LT matrix elements are bounded, so are the eigenvalues $\tilde{J}(\mathbf{k}\nu)$. So if the mode at $\mathbf{Q}_0$ goes unstable at quadratic order in $\delta\mathbf{k}$, there must be higher-order positive terms in the expansion. Thus the single local minimum of $\tilde{J}(\mathbf{k}\nu)$ bifurcates in some fashion. The corresponding spin state cannot be a commensurate spiral, but it might be representable in the framework of planar stackings (Sec. V B).

This technique was used, for example, to analyze how the $\mathbf{Q}_0 = (1/2, 1/2, 0)$ wavevector is destabilized in the LT phase diagram. Simulations had found degenerate antiferromagnetic orderings at that wavevector; if an incommensurate wavevector of form $(q, q, 0)$ had been stabilized, this might have been the basis of a non-coplanar spiral stacked in the $(1, 1, 0)$ direction.

The LT matrix is given by:

$$J_{ii}(\mathbf{k}) = \quad 2J_2 \cos k_i + 2J_2'(\cos k_j + \cos k_k) + 4J_4 \cos k_i \\ \times (\cos k_j + \cos k_k) + 4J_4' \cos k_j \cos k_k \tag{A1a}$$

$$J_{ij}(\mathbf{k}) = \quad 4J_1 \cos\frac{k_i}{2}\cos\frac{k_j}{2} + 8J_3\cos\frac{k_i}{2}\cos\frac{k_j}{2}\cos k_k. \tag{A1b}$$

Here j, k in (A1a) means the indices other than i, similarly k in (A1b) is the index other than i, j. If we substitute $\mathbf{k} = (k, 0, 0)$, for example, the eigenvalues along this cut are

$$\tilde{J}(\mathbf{k}, 0) = -J_2 + 2J_4' - (J_F(0) - J_2)[1 + \cos k] + 2J_X(k); \tag{A2a}$$

$$\tilde{J}(\mathbf{k}, \pm) = -\frac{1}{2}\Big[2J_2' - 4J_4 + (J_F(0) + 4J_4)(1 + \cos k) + 2J_X(k)\Big] \\ \pm \frac{1}{2}\Big\{[(J_2 - J_2' + 2J_4 - 2J_4')(1 - \cos k) + 2J_X(k)]^2 + 16J_X^2(0)(1 + \cos k)\Big\}^{1/2}. \tag{A2b}$$

Along another cut through the zone, $\mathbf{k} = (k, k, 0)/2\sqrt{2}$, the eigenvalues are

$$\tilde{J}(\mathbf{k}, 0) = J_2 - 2J_4' - 2J_F(0)\cos^2 k + 2J_X(0)\cos^2 k; \tag{A3a}$$

$$\tilde{J}(\mathbf{k}, \pm) = J_2' + 2J_4\cos^2 2k - (J_F(2k) + 2J_2' + 4J_4\cos 2k)\cos^2 k - 2J_X(0)\cos^2 k \\ \pm \frac{1}{2}\Big\{[(J_F(2k) - 4J_4'\cos 2k)\sin^2 k - J_X(0)\cos^2 k]^2 + 8J_X(2k)^2\cos^2 k\Big\}^{1/2} \tag{A3b}$$

In both cuts, where $J_F(q) \equiv J_2 + J_2' + 2J_4\cos q + 2J_4'\cos q$ is the effective ferromagnetic coupling and $J_X(q) = J_1 +$

$2J_3 \cos q$ is the effective cross-sublattice coupling.

2. State Perturbation (chain lattice example)

The major advantage of applying perturbation theory to a parametrization of the lattice's spins, rather than the LT matrix, is that it can accomodate a more generic ground state. This is not say that it avoids the disconnect between the state being perturbed and the actual ground state, if the perturbed state does not encompass the true ground state then the disconnect is required. However, this method does allow us to consider states composed of multiple LT wave-vectors.

In the octahedral lattice, most of the ground state types we encountered – even the noncollinear ones – are essentially built using a single "star" of symmetry-related ordering wave-vectors. Therefore, for the octahedral lattice, the actual phase diagram mostly reflects the LT phase diagram and it is preferable to find phase boundaries via the LT perturbation method illustrated above in Sec. A 1. For the chain lattice, however, the ground state is typically characterized by several wave-vectors.

(as noted near the beginning of Sec. V)

Such multi-LT wave-vectors are all parametrized by some form of "conic spirals," a mix of a planar spiral using the wavevector (q) and a deviation along the wavevector (k_2) where k_2 is either integer or half-integer (since the chain lattice is 1D, the wave-vectors are as well). Within a range of parameter space j_1 through j_4/j_4' (j_5 and higher all 0), these conic spirals are the most general form of ground state, making the problem of finding the ground state amenable to variational methods.

As an illustration of determining the ground state by variational methods, we consider the problem of finding the phase boundaries for the "alternating conic" $k_2 = 1/2$. The spin configurations in the lattice are parametrized by Eq.(5.3b). Without loss of generality, we take the odd sites to be the ones with planar spins. A symmetry relates the states (5.3b) to the other family of alternating conic configurations in which even and odd sites have swapped roles, if one also swaps in parameter space $(j_2, j_4) \leftrightarrow (j_2', j_4')$.

Up to interaction j_4, the energy per unit cell is

$$E = -2(j_1 \cos \psi + j_3 \cos 3\psi) \cos \alpha$$
$$- 2(j_2 \cos^2 \psi - j_4 \sin^2 2\psi) \cos^2 \alpha$$
$$+ j_2 - j_4 - j_2' \cos 2\psi - j_4' \cos 4\psi \quad \text{(A4)}$$

Setting $\partial E / \partial(\cos \alpha) = 0$ to minimize (A4), we see that the optimal angle α^*, is given by

$$\cos \alpha^* = -\frac{1}{2 \cos \psi} \frac{j_1 + j_3(4 \cos^2 \psi - 3)}{j_2 - 4 j_4 \sin^2 \psi} \quad \text{(A5)}$$

Notice the symmetry under reversing the signs of j_1 and j_3 and $\alpha \leftrightarrow \pi - \alpha$. Of course, a necessary condition is that the r.h.s. of (A5) lies in $(0, +1)$ (recall that $0 \leq \alpha \leq \pi/2$ by definition), otherwise α^* is pinned to 0 or $\pi/2$, which would

be a planar spiral (or possibly a collinear state, depending on the value of ψ).

Plugging (A5) into Eq. (A4) leaves $\psi = q/2$ as the only variational parameter:

$$E = \frac{2 j_3^2 \left(\frac{j_1 - 3 j_3}{4 j_3} + \cos^2 \psi \right)^2}{j_4 \frac{j_2 - 4 j_4}{4 j_4} + \cos^2 \psi} - j_2' \cos 2\psi -$$
$$- j_4' \cos 4\psi - j_2 - j_4 \quad \text{(A6)}$$

If we drop the secondary couplings equation (A 2) reduces to

$$E = \frac{1}{2} \frac{j_1^2}{j_2} - j_2' \cos 2\psi \quad \text{(A7)}$$

Since (A7) is linear in $\cos 2\psi$, its ground state given by $\psi_m = m\pi/2$, with m integer. If m is odd, then Eq.A7 breaks down, since Eq.(A5) is singular. What actually occurs here is that the sublattices have adopted an antiferromagnetic structure, decoupling the sublattices. Because the sublattices are decoupled, α is arbitrary (representing the freedom the decoupled sublattices to rotate relative to each other). The energy for such a configuration is $E = j_2 + j_2'$. Conversely, if m is even, then the ground state is a splayed state (assuming that $|j_1| < |2j_2|$) That means a commensurate, *planar* state (using the xz plane, or collinear if α^* is trivial). Thus, with only primary couplings, even though the two sublattices are inequivalent, we *cannot* obtain a non-coplanar spiral.

When we turn on (not too large) secondary couplings, those commensurate states will remain stable out to the critical coupling, at which the optimal wavevector bifurcates. Therefore we expand (A 2) in powers of $\delta \equiv \psi - \psi_m$ about both kinds of stationary point [59] to find:

$$E(\delta) = \frac{(j_1 + j_3)^2}{2 j_2} - j_2' - j_4' - j_2 - j_4 +$$
$$[2 \frac{(j_1 + j_3)^2}{j_2^2} j_4 - 4[j_1 - j_3] \frac{j_1}{j_2} + 2 j_2' + 8 j_4'] \delta^2 \quad \text{(A8a)}$$

$$E(\frac{\pi}{2} + \delta) = \frac{1}{2} \frac{[j_1 - 3 j_3]^2}{j_2 - 4 j_4} + j_2' - j_4' - j_2 - j_4 +$$
$$\left(4 \frac{j_1 - 3 j_3}{j_2 - 4 j_4} j_3 + 2[\frac{j_1 - 3 j_3}{j_2 - 4 j_4}]^2 j_4 - 2 j_2' + 8 j_4' \right) \delta^2 \quad \text{(A8b)}$$

The commensurate state becomes unstable to $\delta \neq 0$ when the coefficient of the quadratic term goes negative, so the conditions to induce instability are:

$$E(\delta) : 0 \geq \frac{(j_1 + j_3)^2}{j_2^2} j_4 - 2 \frac{[j_1 - j_3]}{j_2} j_3 + j_2' + 4 j_4' \quad \text{(A9a)}$$

$$E_{\frac{\pi}{2}} : 0 \geq [\frac{j_1 - 3 j_3}{j_2 - 4 j_4}]^2 j_4 + 2 \frac{j_1 - 3 j_3}{j_2 - 4 j_4} j_3 - j_2' + 4 j_4' \quad \text{(A9b)}$$

Combined with the requirement that $|\cos\alpha| < 1$ in (A5), Eqs. (A9) give the minimum necessary conditions for the existance of an alternating conic state.

[1] A.Yoshimori, J. Phys. Soc. Jpn. 14, 807 (1959); J. Villain, J. Phys. Chem. Solids 11, 303 (1959); T. A. Kaplan, Phys. Rev. 116, 888 (1959).

[2] T. A. Kaplan and N. Menyuk, Phil. Mag. 87, 3711 (2006)

[3] C. L. Henley, Phys. Rev. Lett. 62, 2056 (1989).

[4] E. F. Shender, Sov. Phys. JETP, 56, 178 (1982).

[5] C. L. Henley and B. E. Larson, preprint (arxiv 2008); B. E. Larson and C. L. Henley, "Ground State Selection in Type III FCC Vector Antiferromagnets" (unpublished preprint, 1990).

[6] X. G. Wen, F. Wilczek, and A. Zee, Phys. Rev. B 39, 11413 (1989).

[7] S. Sachdev (personal communication).

[8] L. Messio, B. Bernu, and C. Lhuillier, Phys. Rev. Lett. 108, 207204 (2012).

[9] Y. Taguchi, Y. Oohara, H. Yoshizawa, N. Nagaosa, and Y. Tokura, Science 291, 2573 (2001),

[10] A. Kalitsov, B. Canals, and C. Lacroix, J. Phys. Conf. proc. 145, 012020 (2009).

[11] M. Taillefumier, B. Canals, C. Lacroix, V. K. Dugaev, and P. Bruno, Phys. Rev. B 74, 085105 (2006)

[12] N. Nagaosa, J. Sinova, S. Onoda, A. H. MacDonald, and N. P. Ong, Rev. Mod. Phys. 82, 1539 (2010)

[13] C. L. Henley, Ann. Phys. (N. Y.) 156, 368-411 (1984),

[14] S.-W. Cheong and M. Mostovoy, Nature Materials 8, 13 (2007).

[15] T. Kimura, Ann. Rev. Mater. Sci. 37, 387 (2007).

[16] T. Kimura, J. C. Lashley, and A. P. Ramirez, Phys. Rev. B 73, 220401 (2006)

[17] D. Khomskii, Physics 2, 20 (2009).

[18] Y. J. Choi, J. Okamoto, D. J. Huang, et al. K. S. Chao, H. J. Lin, C. T. Chen, M. van Veenendaal, T. A. Kaplan, and S. W. Cheong Phys. Rev. Lett. 102, 067601 (2009).

[19] R. Moessner and J. T. Chalker, Phys. Rev. Lett. 80, 2929 (1998); Phys. Rev. B 58, 12049 (1998).

[20] S. T. Chui, Phys. Rev. B 15, 307 (1977).

[21] P. Reed, J. Phys. A 10, 1745 (1977).

[22] M. Hermele, M. P. A. Fisher, and L. Balents, Phys. Rev. B 69, 064404 (2004).

[23] T. S. Pickles, T. E. Saunders, and J. T. Chalker, EPL 84, 36002 (2008).

[24] R. Shankar, F. J. Burnell, and S. L. Sondhi, Ann. Phys. (N.Y.) 324, 267 (2008).

[25] H. Takizawa, T. Yamashita, K. Uheda, and T. Endo, J. Phys. Condens. Matter 14, 11147 (2002)

[26] D. Fruchart, E. F. Bertaut, J. P. Sénateur, and R. Fruchart, J. de Physique Lett. 38, L-21 (1977); D. Fruchart and E. F. Bertaut, J. Phys. Soc. Jpn. 44, 781 (1978)

[27] T. Koyama, H. Yamashita, Y. Takahashi, T. Kohara, I. Watanabe, Y. Tabata, and H. Nakamura, Phys. Rev. Lett 101, 126404 (2008).

[28] V. H. Tran, W. Miller, and Z. Bukowski, Phys. Rev. Lett. 100, 137004 (2008).

[29] T. Nagamiya, "Helical Spin Ordering: 1 Theory of Helical Spin Configurations", in *Solid State Physics* vol. 20, p. 306, ed. F. Seitz, D. Turnbull, and H. Ehrenreich (Academic Press, New York and London 1967).

[30] J. M. Luttinger and L. Tisza, Phys. Rev. 70, 954 (1946).

[31] D. H. Lyons and T. A. Kaplan, Phys. Rev. 120, 1580 (1960).

[32] J. Samuel Smart, *Effective field theories of magnetism* (W. B. Saunders, Philadelphia, 1966); see chapter 8.

[33] D. Bergman, J. Alicea, E. Gull, S. Trebst, and L. Balents, Nature Physics 3, 487 (2007).

[34] S. Okumura, H. Kawamura, T. Okubo, Y. Motome, J. Phys. Soc. Jpn. 79, 114705 (2010); A. Mulder, R. Ganesh, L. Capriotti, and A. Paramekanti, Phys. Rev. B 81, 214419 (2010).

[35] D. H. Lyons, K. Dwight, T. A. Kaplan, and N. Menyuk, Phys. Rev. 126, 540 (1962).

[36] M. J. Freiser, Phys. Rev. 123, 2003 (1961).

[37] L. R. Walker and R. E. Walstedt, Phys. Rev. Lett. 38, 514 (1977)

[38] C. L. Henley, Ann. Phys. (N. Y.) 156, 324 (1984).

[39] C. L. Henley, Can. J. Phys. 79, 1307 (2001).

[40] V. Elser, I. Rankenburg, and P. Thibault, PNAS 104, 418 (2007).

[41] This is not quite the magnetic structure factor, since that includes interferences between different sublattices.

[42] Occasionally the end-to-end plot is illuminating even in higher dimensions, the sequence of spins being defined by a raster scan that goes down rows – limited to one of the three sublattices – running in one of the coordinate directions.) For example, the double-twist state (Sec. VI) was discovered from common-origin and end-to-end plots.

[43] E. Rastelli, A. Tassi, and L. Reatto, Physical B & C 97, 1 (1979); E. Rastelli and A. Tassi, J. Phys. C: 19, L423 (1986).

[44] J. N. Reimers, A. J. Berlinsky, and A. C. Shi, Phys. Rev. B 43, 865 (1991).

[45] D. H. Lyons and T. A. Kaplan, J. Phys. Chem. Solids, 25, 645 (1964).
H.-J. Schmidt and M. Luban, J. Phys. A 36, 6351 (2003);

[46] J.-C. Domenge, P. Sindzingre, C. Lhuillier, and L. Pierre, Phys. Rev. B 72, 024433 (2005).

[47] J.-C. Domenge, C. Lhuillier, L. Messio, L. Pierre, and P. Viot, Phys. Rev. B 77, 172413 (2008).

[48] Spin configurations on a cuboctahedron were studied by: J. Schulenberg, A. Honecker, J. Schnack, J. Richter, and H.-J. Schmidt, Phys. Rev. Lett. 88, 167207 (2002).

[49] We did not include the asymmetric conic state in table I since we will see that it is only found on the phase boundary between two other states. For the octahedral lattice, then, it appears only as a randomly chosen member of a family of highly degenerate states (using the classification of Sec. II D), rather than a genuine ground state.

[50] Due to the complexity of the double-twist state, the phase boundaries of the double-twist state shown in Figure 6 were *not* generated by variationally optimizing a parametrized Hamiltonian and finding absolute minima. Instead, we show the phase boundary from the "Luttinger-Tisza phase diagram", i.e. the boundary of the region of parameter space in which $(q,q,0)$ was the optimal wave-vector. As argued in Sec. II A, that will produce a phase diagram topologically similar to the true phase diagram.

[51] Around the tricritical-type points where the transition switches from first-order to degenerate, there are alternating conic states only slightly higher in energy than the helimagnetic states, so that a sliver of alternating conic may be spuriously identified here if numerical results are not checked analytically.

[52] L. Messio, C. Lhuillier, and G. Misguich, Phys. Rev. B 83,

184401 (2011).

[53] M. Matsuda, J.-H. Chung, S. Park, T. J. Sato, K. Matsuno, H. Aruga-Katori, H. Takagi, K. Kakurai, K. Kamazawa, Y. Tsunoda, I. Kagomiya, C. L. Henley, and S.-H. Lee, Europhys. Lett. 82, 37006 (2008).

[54] D. Tsuneishi, M. Ioki, and H. Kawamura, J. Phys. Condens. Matter 19, 145273 (2007).

[55] T. Nakamura and D. Hirashima, J. Mag. Mag. Materials 310, 1297 (2007).

[56] G.-W. Chern, R. Moessner, and O. Tchernyshyov Phys. Rev. B 78, 144418 (2008) .

[57] "Ordering of the pyrochlore Ising model with the long-range RKKY interaction" A. Ikeda and H. Kawamura J. Phys. Soc. Jpn. 77, 073707 (2008).

[58] M. Lapa, B.S. thesis, Cornell University (2012); M. Lapa and C. L. Henley, in preparation.

[59] There are just two kinds of stationary point since (A7) has period π.